MNRAS **000**, 1–15 (2022) Preprint 19 May 2022 Compiled using MNRAS LaTeX style file v3.0

Analysis of eight magnetic chemically peculiar stars with rotational modulation

O. Kobzar[1], V. Khalack[1], D. Bohlender[2], G. Mathys[3], M. Shultz[4], D. M. Bowman[5], E. Paunzen[6], C. Lovekin[7], A. David-Uraz[8,9], J. Sikora[10,11], P. Lampens[12], O. Richard[13]

[1]*Département de Physique et d'Astronomie, Université de Moncton, Moncton, N.B., Canada E1A 3E9*
[2]*National Research Council of Canada, Herzberg Institute of Astronomy and Astrophysics, 5071 West Saanich Road, Victoria, BC, Canada V9E 2E7*
[3]*European Southern Observatory, Alonso de Cordova 3107, Vitacura, Santiago, Chile*
[4]*Department of Physics & Astronomy, University of Delaware, 217 Sharp Lab, Newark, DE 19716, USA*
[5]*Institute of Astronomy, KU Leuven, Celestijnenlaan 200D, B-3001 Leuven, Belgium*
[6]*Department of Theoretical Physics and Astrophysics, Masaryk University, Kotlářská 2, 611 37 Brno, Czech Republic*
[7]*Department of Physics, Mount Allison University, Sackville, N.B., Canada E4L 1E6*
[8]*Department of Physics and Astronomy, Howard University, Washington, DC 20059, USA*
[9]*Center for Research and Exploration in Space Science and Technology, and X-ray Astrophysics Laboratory, NASA/GSFC, Greenbelt, MD 20771, USA*
[10]*Department of Physics, Engineering Physics & Astronomy, Queen's University, Kingston, ON, Canada K7L 3N6*
[11]*Department of Physics and Space Physics, Royal Military College of Canada, PO Box 17000 Kingston, ON, Canada K7K 7B4*
[12]*Royal Observatory of Belgium, Ringlaan 3, B-1180 Brussels, Belgium*
[13]*Laboratoire Univers et Particules de Montpellier, Bât 13- CC072, Place Eugène Bataillon, 34095 Montpellier, France*

Accepted ???. Received ???; in original form ???

ABSTRACT

Since the end of 2018, the Transiting Exoplanet Survey Satellite (*TESS*) has provided stellar photometry to the astronomical community. We have used *TESS* data to study rotational modulation in the light curves of a sample of chemically peculiar stars with measured large-scale magnetic fields (mCP stars). In general, mCP stars show inhomogeneous distributions of elements in their atmospheres that lead to spectroscopic (line profile) and photometric (light curve) variations commensurate with the rotational period. We analyzed the available *TESS* data from 50 sectors for eight targets and reduced them in order to minimize instrumental noise. Analysis of the reduced light curves allowed us to determine rotational periods for all eight of our targets. For each star, we provide a phase diagram calculated using the derived period from the reduced light curves and for the available measurements of the disk-averaged longitudinal magnetic field $\langle B_z \rangle$. In most cases, the phased light curve and $\langle B_z \rangle$ measurements show consistent variability. Using our rotation periods, and global stellar parameters derived from fitting Balmer line profiles, and from Geneva and Strömgren-Crawford photometry, we determined the equatorial rotational velocities and calculated the respective critical rotational fractions $v_{\rm eq}/v_{\rm crit}$ (except for HD 77314). We have shown from our sample that the critical rotational fraction decreases with stellar age. This result is in good accordance with the standard hypothesis that mCP stars start losing their angular momentum during their life on the main sequence.

Key words: methods: photometric – stars: magnetic field – stars: rotation – stars: oscillations – stars: fundamental parameters – stars: chemically peculiar – stars: chemically peculiar – stars: individual: HD 10840, HD 22920, HD 24712, HD 38170, HD 63401, HD 74521, HD 77314, HD 86592

1 INTRODUCTION

Chemically peculiar (CP) stars on the upper main sequence (MS) are identified through abnormally strong absorption lines of some chemical elements. In particular ApBp, stars which were classified as CP2 by Preston (1974), are characterized by strong lines of metals such as Si, Cr, Fe, Sr, and rare earth elements. Such peculiarities that occur in stellar atmospheres might be the result of diffusional gravitational settling (Michaud 1970) known as atomic diffusion (Alecian & Stift 2010).

Preston (1974) mentioned that the group of magnetic ApBp stars shows relatively slow rotation comparing to normal stars of A and B spectral types with the same effective temperatures. Magnetic fields detected in ApBp stars (e.g. Bychkov et al. 2003; Buysschaert et al. 2018; Shultz et al. 2022) are thought to have a fossil origin (Neiner et al. 2015) and are known to range in strength from a few hundred G up to a few tens of kG (Aurière et al. 2007; Shultz et al. 2019; Sikora et al. 2019b). The influence of magnetic fields in ApBp stars is quite significant. It prevents rotational mixing and therefore amplifies atomic diffusion (Alecian & Stift 2010) producing an in-

Table 1. Stellar parameters collected from the literature and derived from our analysis of observed data for the ApBp stars studied in this work. Column (1) presents the HD number, column (2) shows the spectral type of each star inferred from recent studies. Columns (3), (4), (5), and (6) provide data for effective temperature and surface gravity collected from the *TESS* Input Catalog (TIC)[1] and derived from fitting the Balmer line profiles respectively. Column (7) and (8) present rotational periods extracted from the literature and derived from the analysis of light curves. Columns (9) and (10), and (11) and (12) show v$\sin i$ and radial velocity inferred from the literature and derived from fitting the Balmer line profiles, respectively.

Name	Spectral type	$T_{\rm eff}$ (K)		$\log g$		Period (d)		v$\sin i$ (km s^{-1})		v$_{\rm r}$ (km s^{-1})	
	SIMBAD	TIC[1]	This study Balmer	TIC[1]	This study Balmer	Published	This study	SIMBAD	This study Balmer	SIMBAD	This study Balmer
HD10840	B9[2]	11663±317	-	4.11±0.07	-	2.097679(7)[6]	2.0976858(2)	35.0±5.0[14]	-	19.4±2.1[21]	-
HD22920	B8II[3]	13800±200	13678±200	-	3.77±0.20	3.9472(1)[7]	3.947225(2)	37.0±5.0[15]	33.0±5.0	18.0±4.0[15]	18.0±3.0
HD24712	A9Vp[4]	7242±129	7290±200	4.18±0.08	4.06±0.20	12.461(1)[8]	12.45862(5)	6.6±0.6[16]	9.0±3.0	23.2±0.4[22]	22.0±2.0
HD38170	B9[5]	10000±280	9470±200	3.80 ± 0.08	3.65±0.20	2.76618(4)[9]	2.766116(2)	65.0±9.0[17]	65.0±3.0	36.3±0.6[22]	33.0±2.0
HD63401	B9[5]	-	13356±200	-	4.06±0.20	2.41(2)[10]	2.414474(1)	52.0±4.0[18]	52.0±4.0	22.0±1.4[22]	26.0±4.0
HD74521	A1Vp[6]	12188±146	10600±200	-	3.47±0.20	7.0501(2)[11]	7.05010(5)	19.0±4.6[19]	18.0±3.0	27.5±1.4[22]	24.0±3.0
HD77314	A2[5]	9253±372	11437±200	3.69±0.10	3.99±0.20	2.86445(8)[12]	2.864325(1)	-	47.0±3.0	-	-4.0±1.0
HD86592	A0[5]	8129 ±145	7804±200	4.18±0.07	3.83±0.20	2.8867[13]	2.88657(3)	16.2±2.0[20]	27.0±5.0	12.7±0.3[20]	13.0±1.0

Note: [1]Stassun et al. (2018, 2019), [2]Renson & Manfroid (1992), [3]Houk & Swift (1999), [4]Abt & Morrell (1995), [5]Cannon & Pickering (1993), [6]Sikora et al. (2019c), [7]Shultz et al. (2022), [8]Bagnulo et al. (1995), [9]David-Uraz et al. (2021), [10]Hensberge et al. (1976), [11]Dukes & Adelman (2018), [12]Bernhard et al. (2020), [13]Babel & North (1997), [14]Bailey & Landstreet (2013), [15]Khalack & Poitras (2015), [16]Sikora et al. (2019a), [17]Royer et al. (2002), [18]Bailey et al. (2014), [19]Wraight et al. (2012), [20]Babel & North (1997), [21]Levato et al. (1996), [22]Gontcharov (2006)

homogeneous redistribution of elements in stellar atmospheres. It is thought that the magnetic field stabilizes the stellar atmosphere, enabling diffusion to play a greater role as compared, for example, to Am stars (Michaud et al. 2015), which are generally not known to host strong, organized fields at their surface. More complex magnetic field geometries were investigated for magnetic CP stars in Magnetic Doppler Imaging (MDI) studies (Kochukhov & Piskunov 2002; Piskunov & Kochukhov 2002) which explain the interrelation between magnetic field and chemical spots for these stars (Kochukhov et al. 2011; Silvester et al. 2017).

In general, the rotational and magnetic dipole axes are not aligned in CP stars, the abundance spots of peculiar metals results in the flux redistribution which is translated to appearance of brightness spots leading to the modulation of light curve by stellar rotation (Krtička et al. 2015). The description of abundance anomalies in ApBp stars is not an easy task considering that an element's abundance does show both horizontal and vertical stratification in their stellar atmospheres (LeBlanc et al. 2015; Khalack et al. 2017; Khalack 2018; Ndiaye et al. 2018; Khalack et al. 2020). The group of mCP stars exhibits variability of spectral line profiles (Krtička et al. 2015), light curves and magnetic field measurements that all appear to be modulated by the stellar rotation period (Samus' et al. 2017). Fainter CP stars have not been identified yet as magnetic since there are no high-quality polarimetric data with high enough signal-to-noise ratio (see for details Donati et al. 1997; Kochukhov et al. 2010, 2018) from which one can detect a significant magnetic field. A complex magnetic field geometry can complicate even more the detection of magnetic field in the faint CP stars.

In this study, we aimed to determine the rotation periods of eight ApBp stars based on the photometric observations provided by the *TESS* mission, and on the available measurements of the mean longitudinal magnetic field. A sample of eight objects was selected for this study through the preliminary analysis of ApBp stars observed by *TESS* during the first cycle of its mission (Kobzar et al. 2020) (see Subsection 2.1 for the details on selection procedure). Considering that the magnetic field structure in ApBp stars is stable over at least decades (Silvester et al. 2017; Shultz et al. 2018), the measurements of the mean longitudinal magnetic field collected for each selected target should vary on the same timescale as the light curve, which allows one to derive or to confirm the period of stellar rotation with high accuracy.

Observations and data reduction are described in Section 2. Results obtained for individual stars from our sample are presented in Section 3. Discussion of the derived results and conclusion follow in Section 4.

2 OBSERVATIONS, DATA REDUCTION AND METHODS

2.1 *TESS* data

The *TESS* space mission was launched on 2018 April 18 in order to detect exoplanets, via high-precision photometry (Ricker et al. 2015). The data produced by this mission are extremely useful, as they allow the study of not only exoplanets, but variable stars as well. Here we are interested in CP stars that show rotational modulation and, in some cases (HD 24712), stellar pulsations (roAp type; Kurtz 1978) in the presence of a magnetic field (Cunha et al. 2019; Holdsworth 2021; Holdsworth et al. 2021). The observing plan for the primary *TESS* mission was to divide the celestial sphere into 26 sectors (with 24°×96° sky area covered by each sector), so that 13 sectors fall on each ecliptic hemisphere, and overlap near the ecliptic poles. The orbital period of the telescope around the Earth is 13.7 d (Gangestad et al. 2013), that corresponds exactly to half the length of the observation of each sector. One year of observation was dedicated to survey each hemisphere. The photometer works in two observing modes: full frame images (FFIs) from CCDs of each camera, whilst target pixel files (TPFs) collect data only from pixels encompassing pre-selected target stars. *TESS* accumulates data with a 30 min (FFIs) cadence for all stars, and with a 2 min (TPFs) cadence for approximately 200,000 objects that were accumulated from the accepted proposals for the primary mission observations (Stassun et al. 2018, 2019). After Cycle 2 the available modes have been expanded to 20 sec (TPFs) cadence and 10 min (FFIs) cadence observations.

We have used *TESS* data produced by the Science Processing Op-

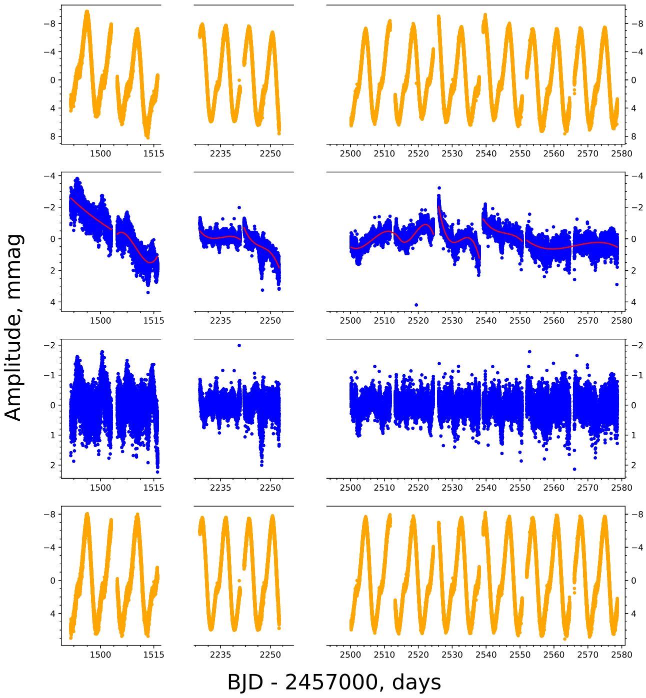

Figure 1. Outline of the detrending procedure of the *TESS* light curve for the star HD 74521. The first panel from the top presents the original light curve, the second panel shows the light curve pre-whitened with the inferred rotational frequency and its harmonic(s) where the red line is residuals once the polynomial fit is subtracted out to remove instrumental distortion, the third panel contains remaining noise with significantly reduced instrumental distortion, the fourth panel presents the final detrended light curve, removing the same polynomial fit as in the previous panel from the original light curve.

erations Center (SPOC)[1] pipeline (Jenkins et al. 2016; Caldwell et al. 2020) and *TESS* light curves[2] which are available from the Mikulski Archive for Space Telescope (MAST)[3] to carry out photometric analysis of selected ApBp stars that are expected to possess a significant magnetic field. Since we are interested only in the ApBp stars that show rotational modulation in their light curves we have selected a sample of eight relatively bright objects ($V < 8.0$ mag) with rotation periods longer than 2 d (see Table 1).

The selected ApBp stars possess relatively small $v \sin i < 65$ km s^{-1}) values (see Table 1) that may indicate the presence of a hydrodynamically stable atmosphere. Meanwhile, fast rotation leads to a mixing in stellar atmosphere that affects or even destroys abundance stratification in the absence of magnetic field. Therefore, we selected for this study stars with rotation periods more than 2 d to ensure the hydrodynamic stability of their stellar atmosphere that is preferred for future analysis of abundance stratification. Knowledge of precise values of rotation periods will help carry out abundance analysis of these stars.

During the selection procedure we have used a database compiled by the TESS-AP procedure (Khalack et al. 2019, 2020) for stars observed by *TESS* with 2 min cadence. This procedure automatically performs a Fourier analysis of the light curves by employing the code PERIOD04 (Lenz & Breger 2005) and collects stellar global parameters from the known astronomical databases (mainly from the *TESS* Input Catalogue (TIC; Stassun et al. 2018, 2019 and SIMBAD[4]). This sample is not complete and includes only 8 interesting targets (see Table 1) selected to test our procedure for data reduction and analysis. Most of the selected targets have been observed in several sectors, which allowed us to effectively reduce their light curves and reduce significantly the instrumental distortions.

The instrumental distortions of a light curve are especially noticeable at the beginning and at the end of every 13.7 d segment of observations, corresponding to the *TESS* orbital period (see, for example, top panel at the Fig. 1). Since all the selected stars exhibit rotational modulation, the first step was to use the code PERIOD04 to detect and extract the frequency of the rotational modulation using pre-whitening method, and its dominant harmonics (no more than three frequencies in total) from the light curve to obtain noisy data with presumably only instrumental distortions (see Fig. 1, second panel from the top). In general, the intervals for approximation were chosen as half length of the observed sector or at the area between the gaps present in the light curve. It is worth emphasizing that at this stage one should choose carefully the intervals used for the polynomial fits, because an insufficient approximation leaves a significant amount of distortion. Meanwhile, an over-correction using a high-order polynomial (more than 3) introduces additional distortion to the light curve, which in turn may lead to a different value of the period of stellar rotation. Then, we approximated the instrumental distortions by a third-order polynomial with the aim to remove them and obtain data generally only with random noise (see Fig. 1, 3rd panel from the top). As the final step, the same polynomials were subtracted from the initial light curve to remove the instrumental distortions and obtain a light curve only with the rotational modulation and the remaining noise (see bottom panel at the Fig. 1). A similar approach was used by Bowman et al. (2018) in the detrending of light curves of ApBp stars from the K2 mission.

We employed Monte Carlo simulations (Bevington 1969) with the code PERIOD04 to determine the precision of defined frequencies which results in high precision of rotational periods. Error bars for the derived phases of the magnetic field measurements include the error of the period estimation. These error bars on the phase are small, given the tight constraints on the rotational periods and, in most cases, the relatively short intervals of time between the magnetic field measurements shown in the phase diagram plots and the derived ephemerides (see Figs. 2, 4, 7, 9, 11, 13, 15 and 17).

2.2 Geneva and Strömgren-Crawford photometry

Geneva and Strömgren-Crawford photometry were used to determine the effective temperature as the first step in evaluation of luminosity by using the method of bolometric correction (BC) (Flower 1996), and radius through the stellar isochrone fitting (Sichevskij 2017). The derived stellar parameters (see Table 2) were employed to determine the ratio $v_{\mathrm{eq}}/v_{\mathrm{crit}}$ for the stars described in this study.

For the Geneva photometry, a General Catalogue of Photometric Data[5] by Paunzen (2015) was used. The values of c1, m1, and (b-y) for the uvbyβ photometry were taken from the Hauck & Mermilliod (1998) catalogue. Unfortunately, one star (HD77314) was left out of consideration because there are no data available for this object. To determine the value of $[u-b]$, we used the original formulae described by Strömgren (1966) as $[u-b] = [c1] + 2[m1]$, where

---

[1] https://archive.stsci.edu/hlsp/tess-spoc

[2] https://archive.stsci.edu/tess/bulk_downloads.html

[3] https://archive.stsci.edu/

[4] http://simbad.u-strasbg.fr/simbad/

[5] https://gcpd.physics.muni.cz/

Table 2. Stellar parameters derived from Strömgren-Crawford photometry ($T_{\rm eff}$ in column 2), from BC (log($L_\star$ in column 4), and from isochrone fitting for the studied stars (columns 3, 6, 8, 10). Data for stellar luminosity, radius and mass inferred from TIC 8 (Stassun et al. 2019) are shown for comparison in column 5, 7, 9 respectively. Data for the derived equatorial velocity are presented in the last two columns.

Name	$T_{\rm eff}$ (K)	$\log g$	$\log(L_\star/L_\odot)$		R ($R_\odot$)		$M_\star$ ($M_\odot$)		logAge	$v_{\rm eq}$ (km s^{-1})	$v_{\rm eq}/v_{\rm crit}$ (%)
HD	This study	This study	This study	TIC	This study	TIC	This study	TIC	This study	This study	This study
	Photometry	Isochrone	BC cor.		Isochrone		Isochrone		Isochrone		
10840	11489 ± 316	4.13(2)	1.97(3)	2.035(35)	2.452(3)	2.550(80)	2.923(1)	3.09(39)	8.224(3)	59.12(7)	12.40(2)
22920	13714 ± 386	3.91(2)	2.65(3)	2.424(320)	3.776(4)	-	4.152(1)	-	8.0734(4)	48.39(5)	10.57(2)
24712	7201 ± 290	4.16(6)	0.85(1)	0.863(15)	1.724(2)	1.715(70)	1.545(1)	1.63(27)	9.03(6)	7.00(1)	1.69(1)
38170	9493 ± 293	3.79(2)	1.94(3)	2.006(34)	3.463(3)	3.354(142)	2.6762(7)	2.56(35)	8.6324(3)	63.32(5)	16.50(2)
63401	13201 ± 380	4.15(2)	2.27(3)	-	2.617(3)	-	3.526(1)	-	7.946(2)	54.82(2)	10.82(2)
74521	10474 ± 285	3.80(2)	2.16(3)	-	3.657(3)	-	3.034(1)	-	8.4811(3)	26.24(2)	6.60(1)
86592	7716 ± 336	4.08(6)	1.10(1)	1.150(23)	2.003(3)	1.895(60)	1.7482(5)	1.981(300)	8.986(2)	35.10(5)	8.61(2)

reddening free indices are calculated $[m1] = m1 + 0.18(b-y)$ and $[c1] = c1 - 0.20(b-y)$. Then, we have used the formulas specified for the stars from CP2 class (Preston 1974) to calibrate the effective temperature

$$\theta_{\rm eff} = 0.234(0.009) + 0.213(0.008)\,[u-b]\ , \tag{1}$$

Netopil et al. (2008) (for the uvbyβ photometry) and

$$\theta_{\rm eff} = 0.835(0.028) + 0.458(0.013)\,(B2-G)^0\ , \tag{2}$$

(Hauck & North 1982) (for the Geneva photometry). Rufener (1988) refers that the standard deviation of colors in the Geneva photometry is around 0.001 mag. The final temperature values are obtained from $\theta_{\rm eff} = 5040/T_{\rm eff}$ (Napiwotzki et al. 1993).

The value of BC is calculated taking into account the coefficients from Flower (1996) and the effective temperature obtained from photometry. For

$$\log(L/L_\odot) = -0.4[M_V - V_\odot - 31.572 + (BC_V - BC_{V,\odot})] \tag{3}$$

we have employed the BC and the magnitude of the Sun which are introduced by Cox (2000) and later adjusted by Torres (2010). To determine the absolute magnitude, we have used values of the derived parallax from Gaia EDR3[6] and apparent magnitude in V band from the Hipparcos catalogue[7].

The Stellar Isochrone Fitting Tool[8] was used to estimate stellar age, radius and mass with the methods described by Sichevskij (2017). Parameters were determined from evolutionary track models of solar metallicity $Z = 0.0152$ (Bressan et al. 2012), according to the given temperature and luminosity. Using the following relation for the equatorial velocity (Netopil et al. 2017)

$$v_{\rm eq}({\rm km s}^{-1}) = 50.579 R(R_\odot)/P({\rm d}) \tag{4}$$

we are able to derive the critical rotational fraction $v_{\rm eq}/v_{\rm crit}$. Considering the formula provided for critical velocity $v_{\rm crit}$ by Georgy et al. (2013), we have derived the following expression for the rotation rate:

$$v_{\rm eq}/v_{\rm crit} = \frac{50.579 R_{\rm eq}/R_\odot}{P}\sqrt{\frac{R_{\rm eq}/R_\odot}{GM_\star/M_\odot}}. \tag{5}$$

Summarising the procedure described above we have collected the data in Table 2 and compared them to the values extracted from the TIC 8 catalogue (Stassun et al. 2018, 2019). The age derived for each target is measured in years (see column 10 of Table 2). The combination of the stellar parameters derived from the analysis of Balmer line profiles, from Geneva and Strömgren-Crawford photometry (see Table 2), and from the literature (see Table 1) in most cases points to the same values considering estimation error bars. Three stars, HD 74521, HD 86592, and HD 10840, fall into exception since HD 74521 shows a big discrepancy for $\log g$ determined from isochrone fitting and TIC catalog, and for $T_{\rm eff}$ in values extracted from the TIC catalog while values derived from Balmer lines and Strömgren-Crawford photometry matched. HD 10840 and HD 86592 overstepped the uncertainties determined for R and $\log(L_\star/L_\odot)$ respectively taking into account the values derived from isochrone fitting and TIC data.

2.3 Spectroscopy

For two stars (HD 22920 and HD 77314) we used also their unpolarized spectra obtained with the spectrograph HERMES (High-Efficiency and high-Resolution Mercator Echelle Spectrograph) at the Mercator telescope on La Palma.

The high-resolution fiber-fed prism-cross-dispersed echelle spectrograph HERMES covers the spectral domain from 3770 Å to 9000 Å in a single exposure with a resolution R = 85000 (Raskin et al. 2011), which is suited for abundance analysis. It is bench-mounted and kept in an environment with the pressure and temperature control to assure the stability of its work. With the HERMES spectrograph, we obtained spectra of HD 22920 and HD 77314 with a relatively high signal-to-noise ratio (SNR $\sim$ 300). The spectra were reduced using the dedicated data reduction pipeline HermesDRS (version 6.0) (Raskin et al. 2011)[9].

2.4 Spectropolarimetry

The spectra have been obtained with the spectropolarimeter ESPaDOnS (Echelle SpectroPolarimetric Device for Observations of Stars) at the Canada-France-Hawaii Telescope (CFHT).

The spectropolarimeter ESPaDOnS[10] is capable of acquiring high resolution (R=65000) Stokes IV spectra in the spectral domain from 3700 Å, to 10000 Å, with high SNR (in our case, spectra of targeted

---

[6] https://gea.esac.esa.int/archive/
[7] https://hipparcos-tools.cosmos.esa.int/HIPcatalogueSearch.html
[8] https://github.com/Johaney-s/StIFT
[9] For more details about this spectrograph and the reduction procedure, see http://www.mercator.iac.es/instruments/hermes/
[10] For more details about this instrument, see http://www.cfht.hawaii.edu/Instruments/Spectroscopy/Espadons/

stars have SNR > 300). The optical characteristics of this spectrograph, as well as their performances, are described by Donati et al. (2006) and Wade et al. (2016). The dedicated software package Libre-ESpRIT (Donati et al. 1997) was employed to reduce the obtained Stokes I spectra and the Stokes V circular polarisation spectra as well.

2.5 Measurements of the mean longitudinal magnetic field.

For each star, the measurements of the hemispherically averaged longitudinal magnetic field $\langle B_z \rangle$ were extracted from the literature or derived from the analysis of available spectropolarimetric observations and are presented in Section 3. The $\langle B_z \rangle$ values (see Table A1) have been derived from analysis of spectra obtained with different instruments (Donati et al. 2006; Bagnulo et al. 2015; Monin et al. 2015) and using different methods (Donati & Collier Cameron 1997; Bagnulo et al. 2002; Kochukhov et al. 2010; Mathys 2017), and may be inconsistent with each other. This information should be considered during analysis of $\langle B_z \rangle$ variability with rotational phase.

We determined the mean longitudinal magnetic field $\langle B_z \rangle$ of HD 24712, HD 63401 and HD 74521 at the various epochs of observation by application of the moment technique to the Stokes IV spectra of these stars that were recorded with ESPaDOnS. The analysis procedure is as described by Mathys (2017). In short, in each spectrum, we measured the first order moments about the central wavelengths λ_0 of the Stokes V profiles of a set of selected diagnostic lines and performed a least-squares fit to derive the value of $\langle B_z \rangle$ from the slope of the linear dependence of these moments on the product of the effective Landé factors of the corresponding transitions by λ_0^2. We used the standard error of the longitudinal field that is derived from this least-squares analysis as an estimate of the uncertainty affecting the obtained value of $\langle B_z \rangle$. For HD 24712, we used Fe I lines as diagnostic lines, and for HD 74521, Fe II lines. Lines of these two ions were systematically used by Mathys (2017) for magnetic field determinations, on account of the fact that inhomogeneities in the distribution of iron over the surfaces of Ap stars tend to be moderate, so that measurements based on the analysis of Fe lines are mostly representative of the intensity and structure of the magnetic field itself. However, for HD 63401, whose $v \sin i$ is higher than for HD 24712 or HD 74521, the Fe lines proved ill-suited for magnetic field determination, so we used Si II lines instead as diagnostic lines. Due to the highly non-uniform distribution of Si on the surface of HD 63401, these lines show considerable distortions, variable with rotation phase, which complicate their measurements. One should keep in mind that the derived $\langle B_z \rangle$ values are representative of the common contribution of the geometrical structure of the magnetic field and of the inhomogeneous distribution of Si.

For HD 77314 and HD 86592, the reported $\langle B_z \rangle$ measurements (see Table A1) have been obtained with the help of dimaPol spectropolarimeter (Monin et al. 2015). This is a Cassegrain spectrograph installed on 1.8-m Plaskett telescope of the Dominion Astrophysical Observatory (DAO). It is used to carry out circular spectropolarimetry of magnetic stars with resolution R~10000 in the 280Å wide spectral region centered on the H_β Balmer line. The spectropolarimeter dimaPol employs hydrogen H_β and metallic lines around it to measure the hemispherically averaged longitudinal magnetic field, and therefore is less effected by rotational broadening and is capable to measure $\langle B_z \rangle$ in stars with relatively large values of vsin$i$ (see for more details Monin et al. 2015).

The timestamps of flux and $\langle B_z \rangle$ measurements were converted to the units of Barycentric Julian Date to use the same time units to plot the light curve and magnetic field phase diagrams.Since the rotation periods obtained from photometric observations were used to build a phase diagram for most stars, the zero phase for the magnetic and photometric data was set at the minimum closest to the beginning of the analysed light curve.

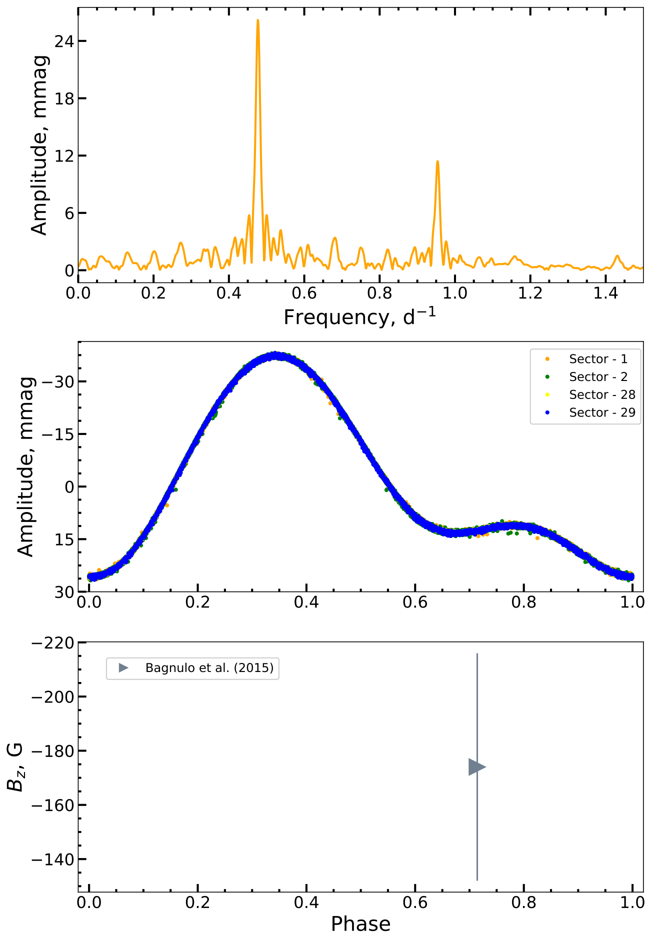

Figure 2. Periodogram (top panel) and phase diagram (bottom panel) built for the rotational period $P = 2.0976858$ d in HD 10840 using the reduced 2 min cadence light curve from the sectors 1 - 2 and 10 min cadence light curve from the sectors 28-29. The $\langle B_z \rangle$ measurement is taken from Bagnulo et al. (2015) (grey triangle).

2.6 Analysis of Balmer line profiles

We used the available high-resolution spectra of the selected targets to estimate their effective temperature and surface gravity, and to measure their radial velocities and vsin$i$ values (see for detail Khalack & LeBlanc 2015). The Stokes I Balmer line profiles (Hβ, Hγ, Hδ, Hϵ, H8, H9, H10, H11, and sometimes H12) and the lines of metals located in the wings of Balmer lines were fitted by the theoretical profiles with the help of FITSB2 code (Napiwotzki et al. 2004) employing the grids of stellar atmosphere models (Husser et al. 2013) calculated using the PHOENIX-16 code (Hauschildt & Baron 1999). The derived values of the global stellar parameters mostly fall into the range of estimation error bars compared to the previously published data (see Table 1) and to the results obtained in this study from the Geneva and Strömgren-Crawford photometry (see Table 2).

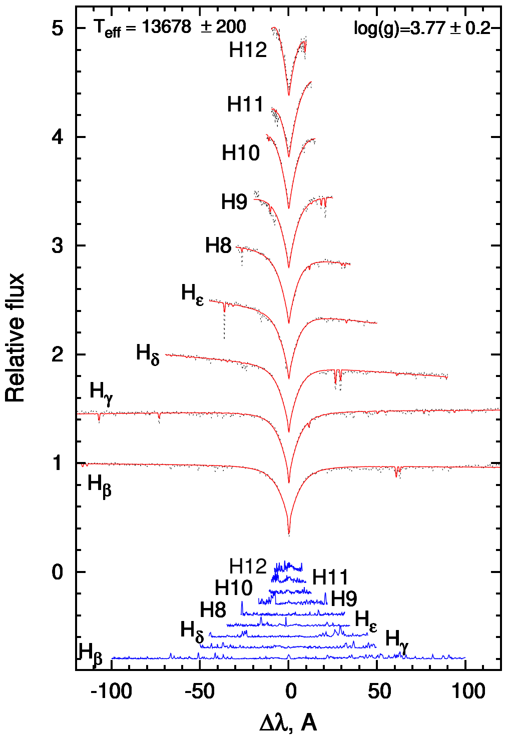

Figure 3. The synthetic spectra (thin dotted lines) are fitting well the Balmer line profiles (thick lines) observed by NARVAL for HD 22920 assuming $T_{\rm eff} = 13678 \pm 200$ K and $\log g = 3.77 \pm 0.2$ and metallicity $M = -0.5$. For the purpose of visual convenience, Balmer lines are shifted by 0.5. Difference between the synthetic and observed spectra is shown by blue lines below.

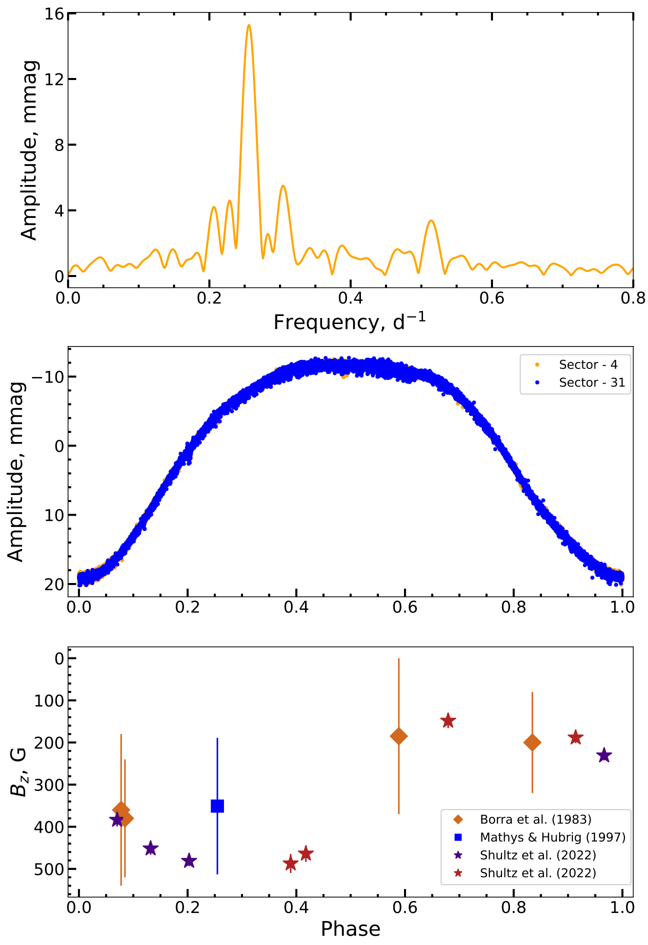

Figure 4. The same as at the Fig 2 but for HD 22920. The phase diagram is built for rotational period 2.947225 d using the reduced light curve obtained from sectors 4 and 31. The measurements of the mean longitudinal magnetic field are taken from Borra et al. (1983) (brown diamonds), Mathys & Hubrig (1997) (blue squares). We show also the LSD measurements of the mean longitudinal magnetic field obtained by Shultz et al. (2022) from NARVAL (red stars) and ESPaDOnS (indigo stars) spectra.

3 RESULTS OF ANALYSIS OF INDIVIDUAL STARS

3.1 HD 10840 (TIC 231844926 = BM Hyi)

According to the catalog of Houk & Cowley (1975) HD 10840 is classified as a CP star of ApSi type and is on the boundary between the spectral types A and B taking into account its effective temperature $T_{\rm eff} = 11600$ K and surface gravity $\log g = 3.60$ (Bailey & Landstreet 2013). Renson & Manfroid (1992) provided for this star a spectral type of B9. Levato et al. (1996) derived radial velocity $v_r = 19.4 \pm 2.1$ km s^{-1} and $v\sin i < 30$ km s^{-1}. Bailey & Landstreet (2013) determined its $v\sin i = 35{\pm}5$ km s^{-1}.

The measurement of the mean longitudinal magnetic field of HD 10840 were obtained by Kochukhov & Bagnulo (2006) and Bagnulo et al. (2015). Kochukhov & Bagnulo (2006) used the method developed by Bagnulo et al. (2002) to derive the mean longitudinal magnetic field from analysis of circular polarisation detected in FORS1 spectra in the area of the Balmer line profiles. Bagnulo et al. (2015) employed the same method to analyze the same FORS1 spectrum of HD 10840, but taking into account the polarisation detected in the Balmer and metal line profiles (see Table A1). Bailey & Landstreet (2013) used a simple magnetic dipole model with the adopted field strength at the magnetic pole, $B_{\rm d}$=500 G, to fit the magnetically sensitive line profiles of Ti, Cr, Fe and Si found in the available spectra of HD 10840.

The period $P = 2.097679(7)$ d of stellar rotation of HD 10840 was determined by Sikora et al. (2019c) from the analysis of photometric data obtained with the space telescope *TESS* in sectors 1-2. In our study, we mesure a more precise value of the rotation period as $P = 2.0976858(2)$ d which is compatible with that from Sikora et al. (2019c). It was derived from the analysis of reduced light curves obtained for this star in sectors 1 and 2 with 2 min cadence and in sectors 28 and 29 with 10 min cadence. The upper panel of Fig. 2 presents a low-frequency region of the discrete Fourier transform of the reduced light curve of HD 10840. From the Fourier analysis we identified a signal at $\nu = 0.47671583(5)$ d^{-1} and its first harmonic. In this case, the derived lower frequency, which appears to be the tallest peak, is identified as the frequency of stellar rotation.The lower panel of Fig. 2 shows the phase diagram built using the derived rotational period and the rotational phase of the available $\langle B_z \rangle$ measurement.

3.2 HD 22920 (TIC 301621458 = FY Eri)

HD 22920 was reported by Cowley et al. (1968) as a variable CP star of spectral type B8pSi, and the most recently determined spectral type is B8II (Houk & Swift 1999). Leone & Manfre (1996) found for this star $T_{\rm eff} = 13800$ K and $\log g = 3.65$, which are close to the estimates of $T_{\rm eff} = 13700$ K and $\log g = 3.72$ obtained by Catanzaro et al. (1999) and to the results $T_{\rm eff} = 13640$ K and $\log g = 3.74$ derived by Khalack & LeBlanc (2015). From the recently obtained ESPaDOnS

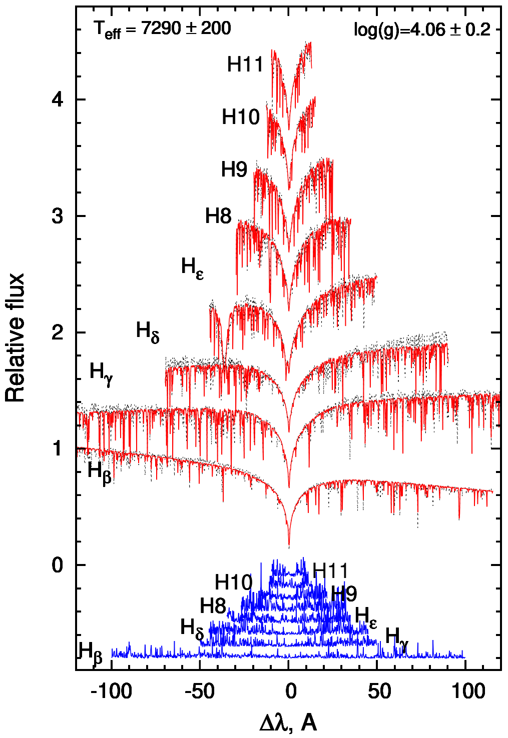

Figure 5. The same as in Fig. 3 but the best fit of Balmer line profiles in HD 24712 is obtained for $T_{\rm eff} = 7290 \pm 200$ K and $\log g = 4.06 \pm 0.2$.

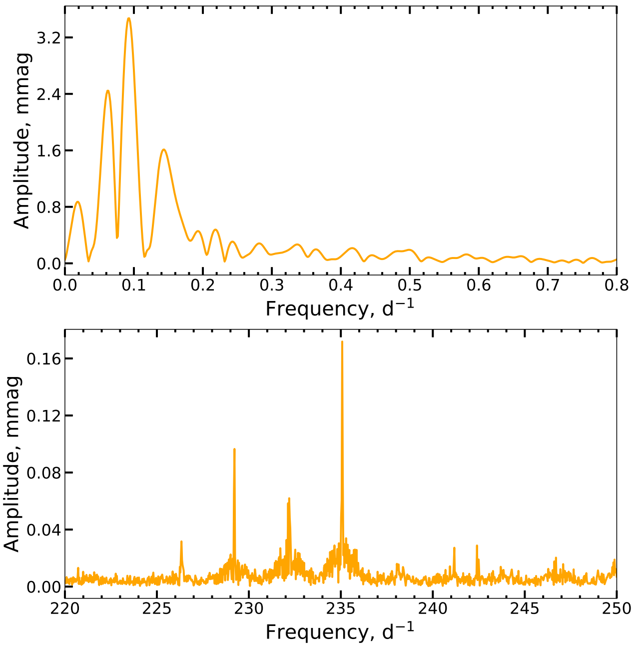

Figure 6. Discrete Fourier transform of the reduced light curve obtained by TEES for HD 24712 in the sector 5 and 31. Significant signals are detected at low frequencies (top panel) that correspond to stellar rotation, and at the high frequencies (bottom panel) that correspond to roAp pulsations.

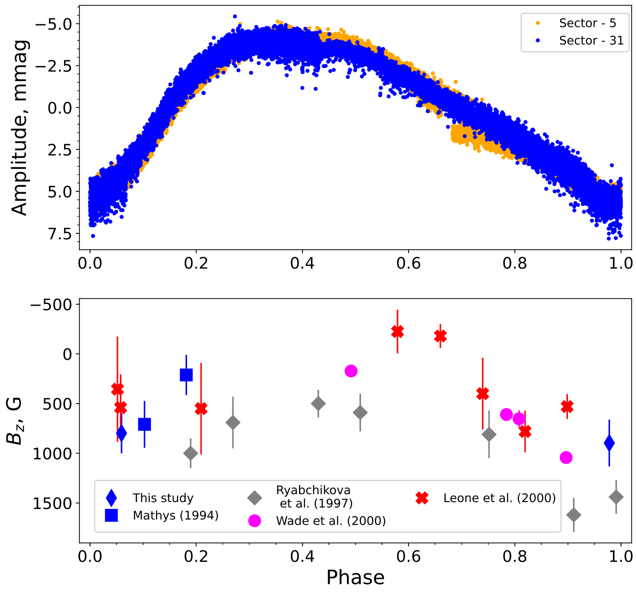

Figure 7. Phase diagram is built using the derived rotational period P = 12.24267 d for the reduced light curve from the sector 5 and 31, and for the $\langle B_z \rangle$ measurement from Wade et al. (2000) (pink circles), Mathys (1994) (blue squares), and Leone et al. (2000) (red cross) obtained for HD 24712.

spectropolarimetric data, we measured the values of $T_{\rm eff} = 13678 \pm 200$ K and $\log g = 3.77 \pm 0.20$ from fitting Balmer line profiles with the help of FITSB2 code (Napiwotzki et al. 2004) (see Fig. 3).

From the analysis of nine Balmer line profiles, Khalack & Poitras (2015) estimated $T_{\rm eff}$= 13640 K and $\log g$ = 3.72. The LTE model of the stellar atmosphere has been calculated by Khalack & Poitras (2015) employing the code PHOENIX (Hauschildt et al. 1997) for the derived effective temperature and $\log g$ to carry out the line profile simulations with the help of ZEEMAN code (Landstreet 1982). The analysis showed that HD 22920 has inhomogeneous abundance distribution of chemical element in its atmosphere.

Mathys & Hubrig (1997) and Borra et al. (1983) analysed spectropolarimetric data obtained by using the Zeeman analyzer at Cassegrain Echelle Spectrograph and photoelectric Pockels cell polarimeter, and derived the mean longitudinal magnetic field in the different rotational phases of HD 22920 (see Table A1). Glagolevskij (2007) calculated the root-mean-square magnetic field (line-of-sight component) $< B_{\rm e} >= 148 \pm 50$ G and average surface magnetic field $B_{\rm s}$ = 800 G. Employing the least-squares deconvolution (LSD) method (Donati & Collier Cameron 1997; Kochukhov et al. 2010) to the available ESPaDOnS and NARVAL spectra of HD 22920, Shultz et al. (2022) measured the mean longitudinal magnetic field (see Table A1) for the additional eight rotational phases and provide precise value for dipolar magnetic filed $B_{\rm d} = 1.6^{+1.1}_{-0.0}$ kG.

Bartholdi (1988) found that this star shows a periodic variability in Geneva 7-color photometry with $P = 3.95$ d. This period is slightly different from the recently published period $P = 3.9489(3)$ d derived from the MASCARA photometric survey (Bernhard et al. 2020), and from the period $P = 3.9472(1)$ d found by Shultz et al. (2022) during the fitting $< B_z >$ measurements. Based on our reduced light curve from the sectors 4 and 31 we have determined the value of the rotation period to be $P = 3.947225(2)$ d for HD 22920 which is in good accordance with the result published by Shultz et al. (2022). The top panel of Fig. 4 shows the discrete Fourier transform of

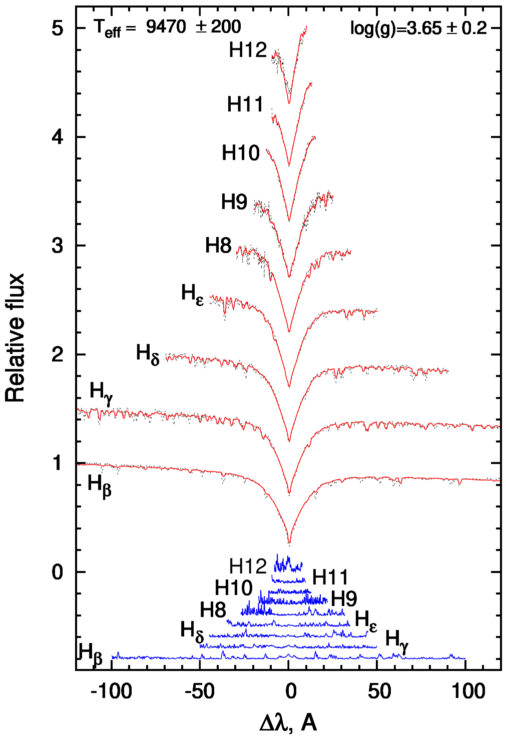

Figure 8. The same type of analysis as in Fig. 3 but the best fit of Balmer lines in HD 38170 is obtained for $T_{\rm eff} = 9470 \pm 200$ K and $\log g = 3.65 \pm 0.2$.

the reduced light curve at low frequencies for HD 22920. We have used the derived period to build a phase diagram of the light curve and magnetic field measurements (see bottom panel of Fig. 4). One can see from the bottom panel of Fig. 4 that the mean longitudinal magnetic field reaches its minimum at the phase $\varphi \simeq 0.3$ when the light curve is close to its maximum, and increases to maximum field at the phase $\varphi \simeq 0.7$ while the light curve is decreasing. It appears that the magnetic field influences the horizontal stratification of the chemical composition in stellar atmosphere of HD 22920, which in turn causes the observed rotational modulation of the light curve assuming the OMR model.

3.3 HD 24712 (TIC 279485093 = DO Eri)

HD 24712 is one of the best-studied rapidly oscillating (roAp) chemically peculiar stars. Abt & Morrell (1995) determined that HD 24712 is a variable star of spectral type A9Vp SrEuCr. Preston (1972) measured for this star the values of $v\sin i = 7.0$ km s^{-1} and $i = 40°$. After Fourier analysis of several Balmer line profiles, Royer et al. (2002) derived $v\sin i = 18.0$ km s^{-1} from the first harmonic. In the study of mCP stars Sikora et al. (2019a) derived measurements of $v\sin i = 6.6 \pm 0.6$ km s^{-1} and $\log g = 3.8 \pm 1.0$ from spectroscopy. Ryabchikova et al. (1997) provide the values of $T_{\rm eff} = 7250$ K and $\log g = 4.2$ from the photometric and spectroscopic observations as well as magnetic measurements. Using available spectroscopic data we determine $T_{\rm eff} = 7290 \pm 200$ K, $\log g = 4.06 \pm 0.20$ and $v\sin i = 22 \pm 2$ km s^{-1} from the analysis of Balmer line profiles (see Fig. 5) which are in a good accordance with the previously published data considering the estimation error bars.

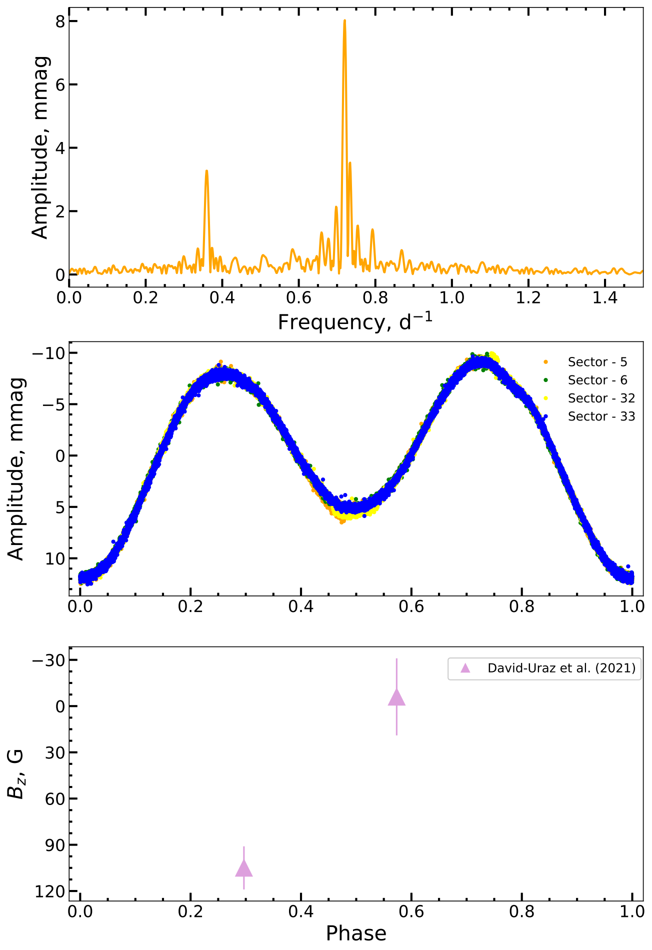

Figure 9. The same as at the Fig 2 but for HD 38170. The phase diagram is built using the rotational period $P = 2.766116$ d derived from the reduced light curve observed in the sector 5, 6, 32 and 33 for the $\langle B_z \rangle$ measurement from David-Uraz et al. (2021) (pink triangle).

The extensive spectroscopic and polarimetric study of HD 24712 by Ryabchikova et al. (2007) determined the phase shifts for the different elements according to the pulsation peak between radial velocity and photometry data which allow estimating the propagation of pulsation maximum. The available measurements of the mean longitudinal magnetic field starting from Preston (1972) up till now are presented in Table A1. Measurements of the mean longitudinal magnetic field were implemented with Zeeman analyzer of the ESO Cassegrain Echelle Spectrograph by Mathys (1994) which measured the wavelength shifts between RC and LC polarizations. Leone et al. (2000) estimated the mean longitudinal magnetic field by using the same method applied to the polarimetric spectra obtained with the fiber-fed REOSC spectrograph of the Catania Astronomical Observatory. Wade et al. (2000) provided the mean longitudinal magnetic field (see Table A1) derived with high-precision from LSD Stokes V profiles by using the MuSiCoS spectropolarimeter observation.

Employing the OMR model, Preston (1972) derived a rotation period of $P = 12.448$ d from metal lines. Later, Kurtz & Marang (1987) improved the estimation of the photometric rotational period to 12.4572(3) d. Using Fourier analysis for measurements of circular and linear polarisation, Bagnulo et al. (1995) derived the period of stellar rotation $P = 12.461(1)$ d which is good accordance with the value obtained by Mathys (1991).

Unlike the other stars in our sample, the detrending procedure for HD 24712 was applied separately to each sector. Since the star demonstrates not only rotational modulation but also pulsations in-

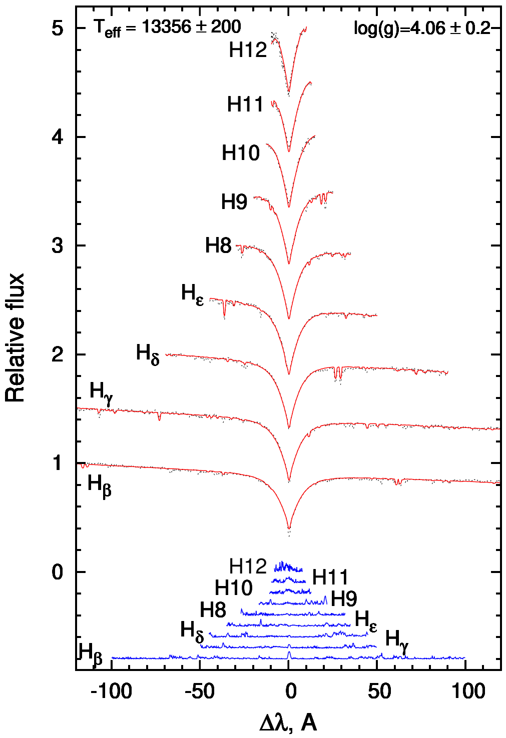

Figure 10. The same type of analysis as in Fig. 3 except for the synthetic lines of the star HD 63401 were used the value of $T_{\rm eff} = 13356 \pm 200$ K and $\log g = 4.06 \pm 0.2$.

herent to the roAp subclass, we performed prewhitening of high-order frequencies of stellar pulsation as well. From Fourier analysis of *TESS* photometric data combined from Sectors 5 and 31, we detected a signal at the frequency (and its first harmonic) that correspond to the period of rotation $P = 12.45862(5)$ d. The top panel in Fig. 6 shows a significant signal detected at the low frequencies of the discrete Fourier transform that is caused by rotational modulation corresponds of the reduced light curve. High-frequency roAp oscillations were discovered in HD 24712 by Kurtz (1981), with the p-mode pulsation being 6.15 min. We have detected p-mode pulsations at high frequencies (see bottom panel in Fig. 6) and we determined the pulsation period $P = 6.1257(1)$ min corresponding to the strongest signal. From the analysis of three frequencies having the most significant amplitudes in the range from 235.07495 $\rm d^{-1}$, 232.19730 $\rm d^{-1}$, 229.20934 $\rm d^{-1}$ we estimated the average separation to be about 2.93281 $\rm d^{-1}$.

3.4 HD 38170 (TIC 140288359 = WZ Col)

HD 38170 has been identified as a CP star with the spectral class B9 by Cannon & Pickering (1993). The radial velocity has been obtained in many studies and are clustered around 35 km $\rm s^{-1}$, but the most recent measurement 36.3 ± 0.6 km $\rm s^{-1}$ has been provided by Gontcharov (2006). From the Fourier transform analysis of line profiles, Royer et al. (2002) derived $v\sin i = 65.0 \pm 9.0$ km $\rm s^{-1}$. Zorec & Royer (2012) derived a stellar mass of $M = 3.07 \pm 0.05 (M_\odot)$, log(Age) = 0.892 ± 0.035 (age measured in Myr), and other fundamental parameters, such as $T_{\rm eff} = 10000 \pm 257$ K and $\log(L_\star/L_\odot) = 2.17 \pm 0.03$, from Strömgren-Crawford photometry.

David-Uraz et al. (2021) confirmed that HD 38170 is magnetic CP star via direct detection in Stokes V profiles obtained with ESPaDOnS (see Table A1) and calculated its dipolar magnetic strength as $B_{\rm d} = 254^{+78}_{-49}$ G by applying a Bayesian analysis on LSD profiles. From the *TESS* first year observations David-Uraz et al. (2021) determined the rotation period $P = 2.76618(4)$ d and by using defined stellar radius, provided $v\sin i = 57 \pm 5$ km $\rm s^{-1}$. The global stellar parameters obtained in this study for HD 38170 are quite similar to those presented by David-Uraz et al. (2021) considering estimation error bars, except for the mass that are lightly different (see Table 4).

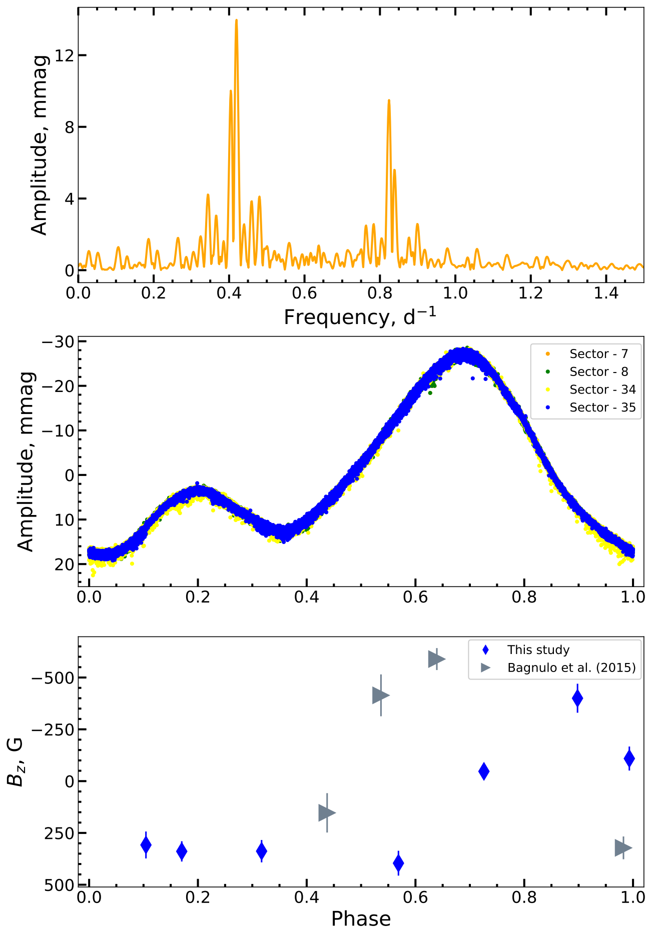

Figure 11. The same as at the Fig 2 but for HD 63401. Phase diagram is built using the derived rotational period $P = 2.414474$ for the reduced light curve from the sectors 7,8, and 34,35 and for $< B_z >$ measurements from Bagnulo et al. (2015) (black triangles).

From the *TESS* observations we were able to identify the rotational period for HD 38170. From Fourier transform analysis (see Fig. 9) we defined a signal at the low-frequency region that may be interpreted as the first harmonic. We have reduced the light curve of this star obtained by TESS in sectors 5, 6, 32 and 33, and phased it with the period of stellar rotation (see the lower panel of Fig. 9). On the phase diagram, one can clearly see two maxima that most probably appear due to the presence of abundance spots in the stellar atmosphere of HD 38170. Contrary to the case of HD 10840 (see Subsection 3.1), the highest peak for HD 38170 is found at larger frequency (second one) which we considered as the fundamental frequency. The rotational period 2.766116(2) d determined for this frequency is consistent with the result derived by David-Uraz et al. (2021).

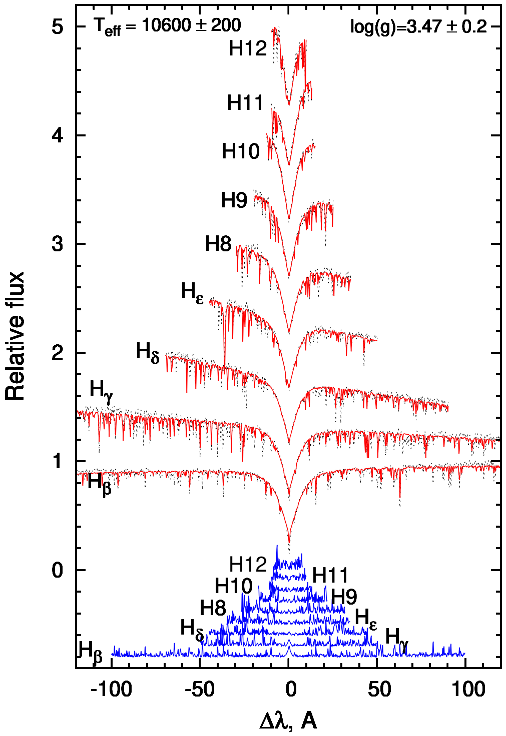

Figure 12. The same as in Fig. 3 but for best fit of Balmer lines in HD 74521 obtained for $T_{\rm eff} = 10600 \pm 200$ K and $\log g = 3.47 \pm 0.2$.

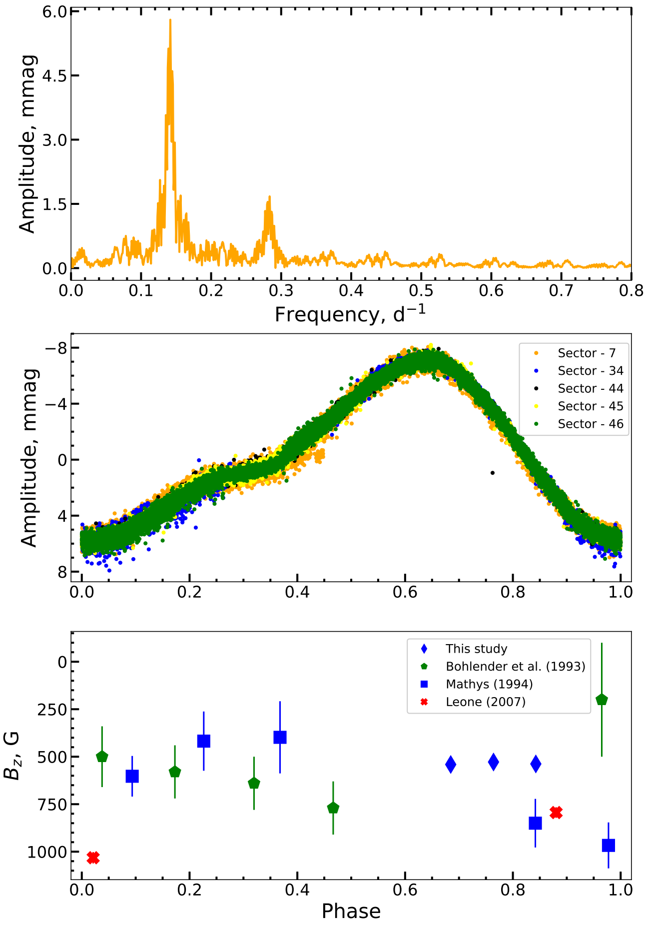

Figure 13. The same as at the Fig 2 but for HD 74521. Phase diagram is built using the derived rotational period $P = 7.05010$ d for the reduced light curve from the sectors 7, 34 and 44 to 46 and for the $\langle B_z \rangle$ measurements from Bohlender et al. (1993) (green pentagons), Mathys (1994) (blue squares and diamonds (private)) and Leone (2007) (red stars).

3.5 HD 63401 (TIC 175604551 = OX Pup)

The star HD 63401 was classified as a variable star of spectral type B9 (Cannon & Pickering 1993). Bailey et al. (2014) provided for HD 63401, $T_{\rm eff} = 13500 \pm 500$ K which was previously mentioned by Landstreet et al. (2007), and derived $\log g = 4.20 \pm 0.20$ and $v\sin i = 52.0 \pm 4.0$ km s^{-1} from the analysis of two FEROS spectra. The radial velocity $v_r = 22.0 \pm 1.4$ km s^{-1} (see Table 1) was derived for HD 63401 by Gontcharov (2006). We report for HD 63401 similar stellar parameters $T_{\rm eff} = 13356 \pm 200$ K, $\log g = 4.06 \pm 0.20$, $v_r = 26.0 \pm 2.0$ km s^{-1} and $v\sin i = 52.0 \pm 4.0$ km s^{-1} obtained from the fitting of Balmer line profiles in the available ESPaDOnS spectra (see Fig. 10).

Glagolevskij (2007) studied HD 63401 and determined the mean effective magnetic field (line-of-sight component) $< B_e >= 70 \pm 50$ G and the root-mean-square magnetic field $B_{\rm rms} = 400$ G. Landstreet et al. (2007) derived the value $B_{\rm rms} = 365$ G, which is in good accordance with the result obtained by Glagolevskij (2007). Bagnulo et al. (2015) used polarimetric spectra obtained with the spectrograph FORS1, and estimated the mean longitudinal magnetic field from the analysis of circular polarisation in the Balmer line profiles and metal lines (see first column in Table A1).

The period of stellar rotation 2.41 ± 0.02 d was derived from the analysis of the light curves observed by the ESO telescope and reported for the first time by Hensberge et al. (1976). From the available photometric TESS data, we confirm the value of the above period. The top panel of the Fig. 11 presents the discrete Fourier transform of the reduced light curve observed by *TESS* in sectors 7, 8, 34 and 35. The significant signals detected at low frequency and its first harmonic may be caused by stellar rotation with the period $P = 2.414474(1)$ d. At the bottom panel in Fig. 11, we show the phase diagram for the reduced light curve together with the phase diagram for the available $< B_z >$ data.

3.6 HD 74521 (TIC 443995718 = BI Cnc)

Abt & Morrell (1995) provided the spectral type A1Vp for HD 74521 with HgMnSiEu strong lines and CaMg weak lines, and $v\sin i = 10$ km s^{-1}. Royer et al. (2002) used Fourier transform analysis of line profiles in the range 420-460 nm to combine the set of rotational velocities for Ap stars on the base of the previous study of Abt & Morrell (1995), and derived for HD 74521 $v\sin i = 18.0 \pm 0.9$ km s^{-1}. Gontcharov (2006) provided the value of radial velocity $v_r = 27.5 \pm 1.4$ km s^{-1}. Wraight et al. (2012) provided for HD 74521 an effective temperature of $T_{\rm eff} = 10789 \pm 500$ K, $v\sin i = 19 \pm 4.6$ km s^{-1}. Our estimates of $T_{\rm eff} = 10600 \pm 200$ K derived from the fitting of Balmer lines (see Fig. 12) and $T_{\rm eff} = 10474 \pm 285$ K inferred from the Strömgren-Crawford photometry (see Table 2) are consistent with the results of Wraight et al. (2012) considering the estimated uncertainties. Also, from the analysis of Balmer line profiles we have obtained $v\sin i = 18 \pm 3$ km s^{-1} and $v_r = 24 \pm 3$ km s^{-1} that are in good accordance with the previously published data taking into account the estimation error bars (see Table 1).

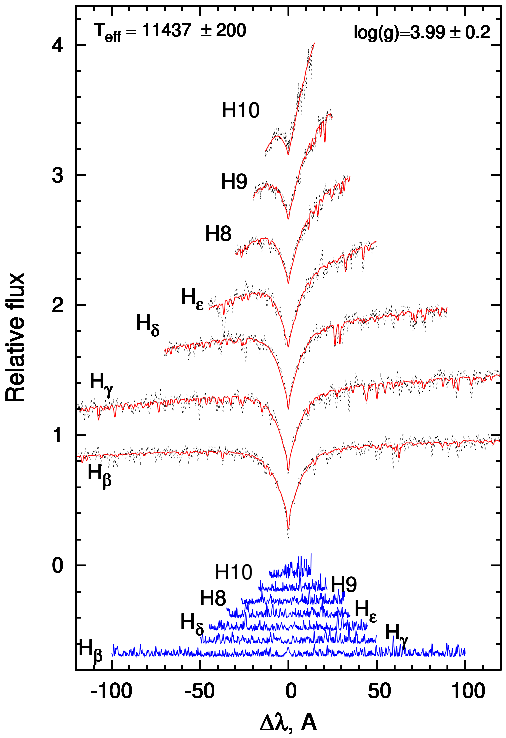

Figure 14. The same type of analysis as in Fig. 3 except for the synthetic lines of the star HD 77314 were used the value of $T_{\rm eff} = 11437 \pm 200$ K and $\log g = 3.99 \pm 0.20$.

HD 74521 was investigated as a mCP star since Stepien (1968) who measured the period of stellar rotation to be $P = 5.43$ d. During the last decades, many rotation periods were derived for HD 74521 from terrestrial and space observations. Recent measurements have been obtained by Leone (2007) as $P = 7.0486(5)$ d, $P = 6.91(1)$ d by Wraight et al. (2012) and $P = 7.0501(2)$ d by Dukes & Adelman (2018).

TESS has carried out observations of HD 74521 in sectors 7, 34 and 44 to 46, which provide a valuable time baseline of almost 3 yr. From the discrete Fourier transform of the reduced light curve, we confirm the value of the rotational period to be $P = 7.05010(5)$ d for HD 74521. The top panel of Fig. 13 shows a significant signal at $\nu = 0.1418419(1)$ d^{-1} that is related to stellar rotation. The bottom panel of Fig. 13 presents a phase diagram. The measurements of the mean longitudinal magnetic field are taken from Bohlender et al. (1993), Mathys (1994) and Leone (2007). The mean longitudinal magnetic field was measured with the Pockels cell polarimeter and the Zeeman analyzer at Cassegrain Echelle Spectrograph respectively. Leone (2007) measured the mean longitudinal magnetic field across the whole spectrum and through Balmer lines obtained with the spectropolarimeter ISIS. The $\langle B_z \rangle$ measurements seem to be correlated with the light curve phase diagram and are reaching their extremum at the minimum of the phased light curve (see bottom panel of Fig. 13).

3.7 HD 77314 (TIC 270487298 = NP Hya)

HD 77314 is a CP star of spectral type A2 (Cannon & Pickering 1993), or alternative type ApSrCrEu (Houk & Swift 1999). The *TESS* input catalogue (TIC) provides the effective temperature $T_{\rm eff} = 9253 \pm 372$ K and surface gravity $\log g = 3.69 \pm 0.10$ (Stassun et al. 2018, 2019). From the fitting of Balmer line profiles in the HERMES spectra (see Fig 14) we have derived $T_{\rm eff} = 11437 \pm 200$ K and $\log g = 3.99 \pm 0.20$ (see Tables 1, 2). As there was no data available in the Geneva and Strömgren-Crawford photometry catalogs, we could not confirm any of the above data, which are in stark disagreement.

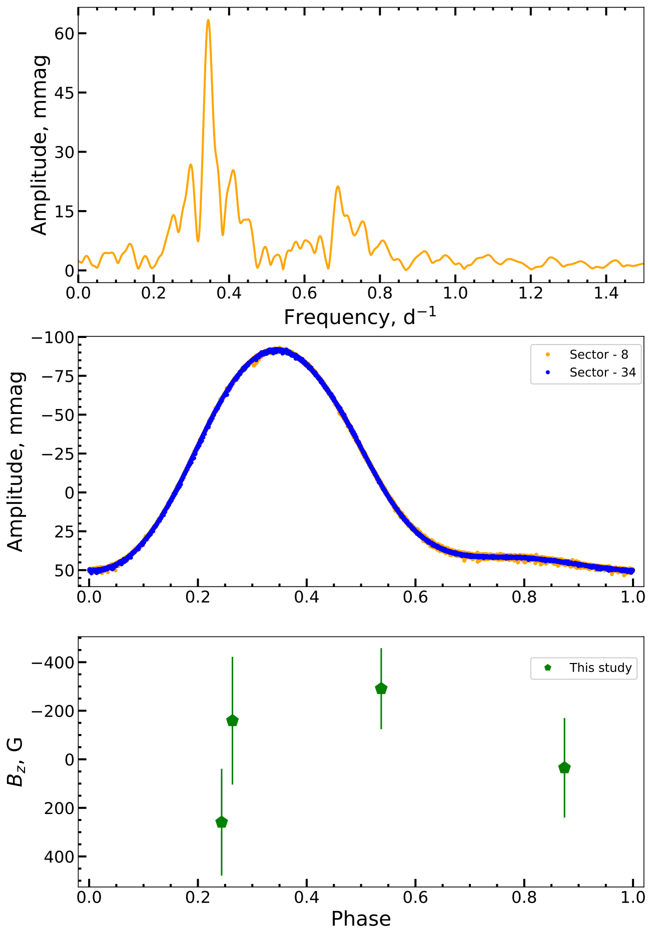

Figure 15. The same as at the Fig 2 but for HD 77314. Phase diagram is built using the derived rotational period $P = 2.864325$ for the reduced light curve from the sectors 8 and 34 and for $< B_z >$ DAO longitudinal magnetic field measurements (green pentagons).

From the extensive study of rotational periods from MASCARA data, Bernhard et al. (2020) derived the rotation period of $P = 2.86445(8)$ d which is in a good accordance with the period of $P = 2.8646$ d presented in the International Variable Star Index of the American Association of Variable Star Observers (VSX; Watson et al. 2006). From the discrete Fourier transform of the reduced light curve observed in sectors 8 (2 min cadence) and 34 (10 min cadence) (see top panel Fig 15) we have detected the signals in the low-frequency region that most probably correspond to rotation period $P = 2.864325(1)$ d which is in good accordance with period determined by Bernhard et al. (2020). In the bottom panel of Fig 15, we provide the phase diagram built with this period for the reduced light curve and for the measurements of the mean longitudinal magnetic field. Considering the obtained error bars the derived $\langle B_z \rangle$ measurements appear to be not so different from zero. We need to use Stokes I and V spectra with higher signal to noise ratio for HD 77314 to measure its magnetic field with high precision.

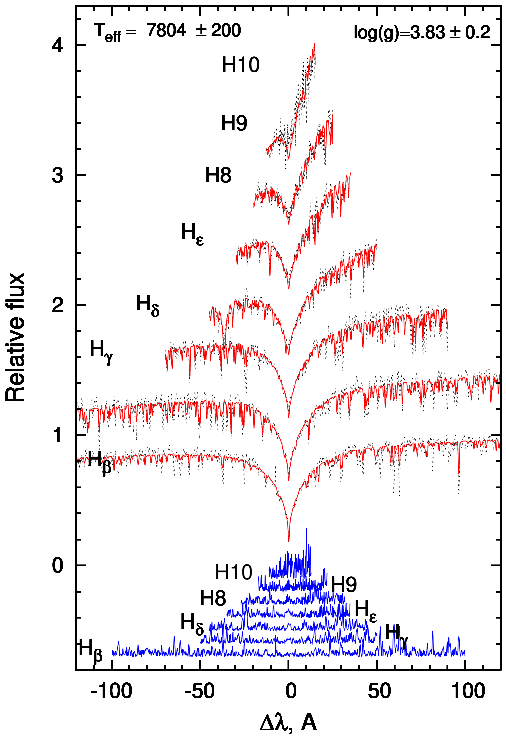

Figure 16. The same as in Fig. 3 but for best fit of Balmer lines in HD 86592 obtained for $T_{\rm eff} = 7804 \pm 200$ K and $\log g = 3.83 \pm 0.20$.

3.8 HD 86592 (TIC 332654682 = V359 Hya)

Houk & Smith-Moore (1988) determined the spectral type of HD 86592 as ApSrEuCr. In this study, the effective temperature $T_{\rm eff} = 7804 \pm 200$ K and surface gravity $\log g = 3.83 \pm 0.2$ are estimated for HD 86592 from the fitting of Balmer line profiles observed with HERMES (see Fig. 16). Considering the estimated uncertainties these data are consistent with the values of $T_{\rm eff} = 7955 \pm 95$ K and $\log g = 4.28 \pm 0.18$ from Kordopatis et al. (2013) and to our estimates of $T_{\rm eff} = 7716 \pm 336$ K and $\log g = 4.08 \pm 0.06$ obtained for this star from the Geneva photometry (see Table 2).

The presence of a strong magnetic field did not allow Babel & North (1997) to estimate the value of rotational velocity from individual line profiles, therefore, they used the correlation dip and derived the values $v_r = 12.7 \pm 0.3$ km s^{-1} and $v\sin i = 16 \pm 2.0$ km s^{-1} for HD 86592. Our estimate of the radial velocity $v_r = 13.3 \pm 1.0$ km s^{-1} is in a good accordance with the published value, while $v\sin i = 27 \pm 5.0$ km s^{-1} appears to be overestimated due to the magnetic widening of line profiles. The study of magnetic fields of cool CP stars leads Babel & North (1997) to discover the strong magnetic field in HD 86592. Measurements of the mean longitudinal magnetic field have been carried out using the cross-correlation method applied to the analysis of ELODIE spectra. These authors also measured a value of the quadratic magnetic field $\langle H^2 \rangle = 15.5 - 16.1$ kG by method described in Mathys (1995).

From the analysis of the discrete Fourier transform of the reduced light curve observed by *TESS* in sectors 8 and 35 we have derived for HD 86592 a rotation period of $P = 2.88657(3)$ d (top panel in Fig. 17). The obtained period coincides with the period P= 2.8867 d provided by Babel & North (1997) from photometric measurements carried out in the Geneva system. In the bottom panel of Fig. 17, we provide the reduced light curve and the measurements of the mean longitudinal magnetic field phased with the period of stellar rotation $P = 2.88657(3)$ d derived for HD 86592 in this study. The available measurements of $\langle B_z \rangle$ have been obtained with the help of dimaPol spectropolarimeter (Monin et al. 2015) and resulted in the period $P = 2.887424$ d which is very close to the one derived from the *TESS* photometry. In the bottom panel of Fig. 17, one can see that the mean longitudinal magnetic field reaches a probable extremum at the phase $\varphi = 0.3$ which is quite close to the maximum of the reduced light curve ($\varphi = 0.4$).

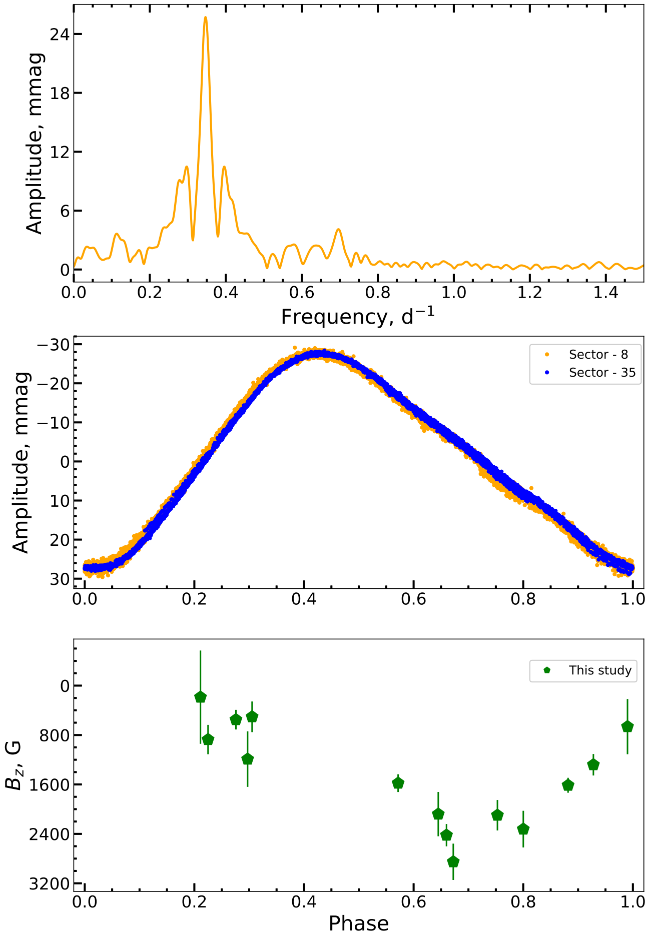

Figure 17. The same as at the Fig. 2 but for HD 86592. Phase diagram is built using the derived rotational period $P = 2.88657$ for the reduced light curve from the sectors 8 and 35 and for $< B_z >$ DAO longitudinal magnetic field measurements(green pentagons).

4 DISCUSSION

We carried out analysis of eight Ap stars with the purpose to determine rotation periods from the recently conducted observations with the NASA *TESS* space telescope and confirm the existence of rotational modulation by comparing phased light curve with the magnetic field measurements phased with the same period. Thus we have collected all available data for each star from the MAST database up to 50 sectors at this moment. We have also collected all available measurements of the mean longitudinal magnetic field $\langle B_z \rangle$ for each star (see Table A1), and phased them according to the derived period. Based on the obtained data and the detrended light curves

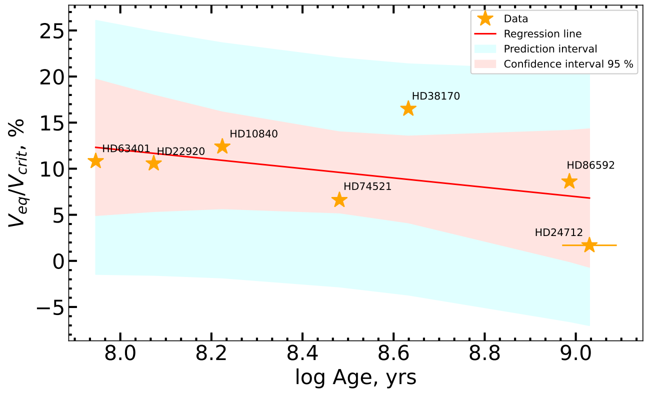

Figure 18. Rotational rates $v_{\rm eq}/v_{\rm crit}$ as a function of age (upper panel) for the seven studied stars (see Tab.2).

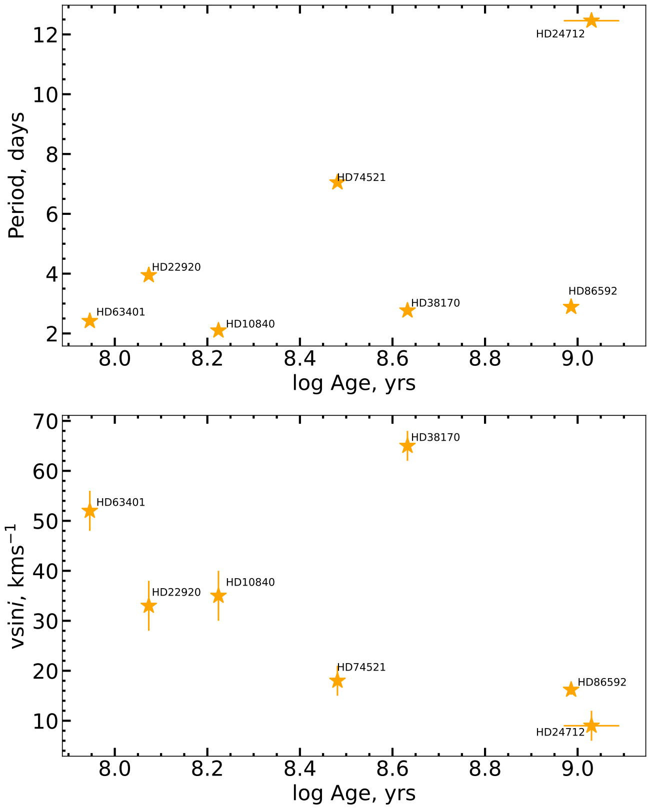

Figure 19. Rotational period (upper panel) and vsin$i$ (lower panel) as a function of age for selected sample (see Tab. 2).

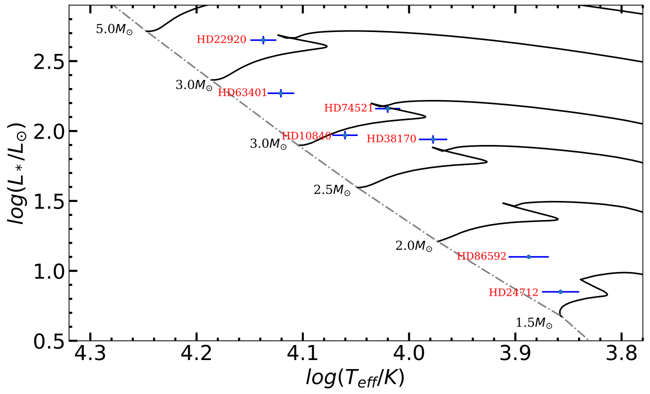

Figure 20. Hertzsprung–Russell diagram diagram built for 7 stars from the studied sample. Evolutionary tracks are calculated for stars of 1.5-5.0 $M_\odot$ assuming solar metallicity without rotation (the continuous lines) starting from the zero age main sequence (dotted line) (Ekström et al. 2012).

one can admit that the periods derived in this study coincide with those previously mentioned in the literature. Nevertheless, our results are obtained with a much higher accuracy provided by much larger timescale of analyzed data.

A dependence of the rotational rate $v_{\rm eq}/v_{\rm crit}$ on stellar age is presented in Fig. 18. This figure shows clearly a decrease of the critical rotational fraction $v_{\rm eq}/v_{\rm crit}$ with the stellar age. We have presented the prediction interval that describes deviation of our estimates of rotational rates from their least square linear approximation. The data may overcome the confidence interval (Cosma 2019), nevertheless, in our case, except for HD 38170 the rest of the sample fall within the confidence interval (see pink area in Fig. 18). Despite the small sample used for analysis, the obtained result is statistically significant. The derived decrease of the ratio $v_{\rm eq}/v_{\rm crit}$ with the stellar age means that younger magnetic stars rotate faster than older ones.

Fig. 19 presents a dependence of the rotational period (top panel) and vsin$i$ (bottom panel) on the stellar age. While the derived periods of stellar rotation are spread from 2 d to 12 d (see top panel of Fig. 19 where, for example, HD 24714 and HD 86592 have a similar relatively large age), the measured values of vsin$i$ show a tendency to decrease with the stellar age (except for HD 38170, see bottom panel of Fig. 19). These data argues in favour of loss of the angular momentum by the magnetic ApBp stars with their age even if some targets from our sample possess different rotational periods at the similar age.

Our finding is in a good agreement with the works of Abt (1979) and Wolff (1981) arguing that the magnetic ApBp stars start losing their angular momentum after they reach the main sequence. Recent studies of Shultz et al. (2019) have confirmed a slow down of stellar rotation of early Bp stars with age, and associate this with magnetospheric braking.

In this paper, we aimed to test the detrending methods applied to the light curves with rotational modulation provided by *TESS* for a sample of magnetic ApBp stars with a fairly wide range of global stellar parameters (see Tables 1 & 2). One of our selected targets, HD 24712, does show high-overtone stellar pulsations of roAp type. To illustrate the diversity of the global stellar parameters we built a Hertzsprung Russell diagram for 7 targets from our sample (see Fig. 20) by using their derived values of effective temperature and luminosity, and by overlapping with evolutionary curves of solar metallicity $Z = 0.014$ without rotation for stars with 1.5-5.0 $M_\odot$ (Ekström et al. 2012). Discrete Fourier transform of the detrended light curves and available measurements of the mean longitudinal magnetic field (see Table A1) allowed us to derive with high-precision periods of stellar rotation for the selected targets, which are in a good accordance with the previously published data (see. Section 3). Analysis of the stellar global parameters derived from the fitting of Bamer line profiles (see Tables 1) and from the Strömgren-Crawford photometry (see Tables 2) resulted in detection of clear decrease of the rotational rate $v_{\rm eq}/v_{\rm crit}$ with stellar age (see Fig. 18) indicating the loss of angular momentum of ApBp stars with their evolution on the main sequence (Abt 1979; Wolff 1981). To improve the statistics of this finding we plan to expand significantly the sample of magnetic CP stars with rotational modulation using the photometric data provided by *TESS* and hopefully by the space telescope *PLATO* as well.

ACKNOWLEDGMENTS

O.K. and V.K. are thankful to the Faculté des Études Supérieures et de la Recherch and to the Faculté des Sciences de l'Université de Moncton for the financial support of this research. V.K. and C.L. acknowledge support from the Natural Sciences and Engineering Research Council of Canada (NSERC). A.D.-U. is supported by NASA under award number 80GSFC21M0002. D.M.B. gratefully acknowledges a senior postdoctoral fellowship from the Research Foundation Flanders (FWO) with grant agreement no. 1286521N. This paper includes data collected with the TESS mission, obtained from the MAST data archive at the Space Telescope Science Institute (STScI). Funding for the TESS mission is provided by the NASA Explorer Program. STScI is operated by the Association of Universities for Research in Astronomy, Inc., under NASA contract NAS 5–26555. We thank the *TESS* and TASC/TASOC teams for their support of the present work. This research has made use of the SIMBAD database, operated at CDS, Strasbourg, France. Some of the data presented in this paper were obtained from the Mikulski Archive for Space Telescopes (MAST). STScI is operated by the Association of Universities for Research in Astronomy, Inc., under NASA contract NAS5-2655. Part of the analysed spectra has been obtained with the spectropolaimeter ESPaDOnS at the Canada-France-Hawaii Telescope (CFHT) which is operated by the National Research Council of Canada, the Institut National des Sciences de l'Univers of the Centre National de la Recherche Scientifique of France, and the University of Hawaii. Part of the used spectra has been aquired with the spectropolaimeter NARVAL at the Télescope Bernard Lyot operated by the Observatoire Midi Pyrénées. Some of the spectra have been obtained with the Mercator Telescope, operated on the island of La Palma by the Flemmish Community, at the Spanish Observatorio del Roque de los Muchachos of the Instituto de Astrofísica de Canarias. The work of the HERMES spectrograph is supported by the Research Foundation - Flanders (FWO), Belgium, the Research Council of KU Leuven, Belgium, the Fonds National de la Recherche Scientifique (F.R.S.-FNRS), Belgium, the Royal Observatory of Belgium, the Observatoire de Genéve, Switzerland and the Thüringer Landessternwarte Tautenburg, Germany.

REFERENCES

Abt H. A., 1979, ApJ, 230, 485

Abt H. A., Morrell N. I., 1995, ApJS, 99, 135

Alecian G., Stift M. J., 2010, A&A, 516, A53

Aurière M., et al., 2007, A&A, 475, 1053

Babel J., North P., 1997, A&A, 325, 195

Bagnulo S., Landi Degl'Innocenti E., Landolfi M., Leroy J. L., 1995, A&A, 295, 459

Bagnulo S., Szeifert T., Wade G. A., Landstreet J. D., Mathys G., 2002, A&A, 389, 191

Bagnulo S., Fossati L., Landstreet J. D., Izzo C., 2015, A&A, 583, A115

Bailey J. D., Landstreet J. D., 2013, A&A, 551, A30

Bailey J. D., Landstreet J. D., Bagnulo S., 2014, A&A, 561, A147

Bartholdi P., 1988, in Halbwachs J. L., Jasniewicz G., Egret D., eds, Détection et Classification des Étoiles Variables. pp 77–83

Bernhard K., Hümmerich S., Paunzen E., 2020, MNRAS, 493, 3293

Bevington P. R., 1969, Data reduction and error analysis for the physical sciences. McGraw-Hill (New York)

Bohlender D. A., Landstreet J. D., Thompson I. B., 1993, A&A, 269, 355

Borra E. F., Landstreet J. D., Thompson I., 1983, ApJS, 53, 151

Bowman D. M., Buysschaert B., Neiner C., Pápics P. I., Oksala M. E., Aerts C., 2018, A&A, 616, A77

Bressan A., Marigo P., Girardi L., Salasnich B., Dal Cero C., Rubele S., Nanni A., 2012, MNRAS, 427, 127

Buysschaert B., Neiner C., Martin A. J., Aerts C., Bowman D. M., Oksala M. E., VanÂ Reeth T., 2018, MNRAS, 478, 2777

Bychkov V. D., Bychkova L. V., Madej J., 2003, A&A, 407, 631

Caldwell D. A., et al., 2020, Research Notes of the American Astronomical Society, 4, 201

Cannon A. J., Pickering E. C., 1993, VizieR Online Data Catalog, p. III/135A

Catanzaro G., Leone F., Catalano F. A., 1999, A&AS, 134, 211

Cosma R., 2019, The Truth about Linear Regression

Cowley A. P., Cowley C. R., Hiltner W. A., Jaschek M., Jaschek C., 1968, PASP, 80, 746

Cox A. N., 2000, Allen's astrophysical quantities

Cunha M. S., et al., 2019, MNRAS, 487, 3523

David-Uraz A., et al., 2021, MNRAS, 504, 4841

Donati J. F., Collier Cameron A., 1997, MNRAS, 291, 1

Donati J. F., Semel M., Carter B. D., Rees D. E., Collier Cameron A., 1997, MNRAS, 291, 658

Donati J. F., Catala C., Landstreet J. D., Petit P., 2006, in Casini R., Lites B. W., eds, Astronomical Society of the Pacific Conference Series Vol. 358, Solar Polarization 4. p. 362

Dukes Robert J. J., Adelman S. J., 2018, PASP, 130, 044202

Ekström S., et al., 2012, A&A, 537, A146

Flower P. J., 1996, ApJ, 469, 355

Gangestad J. W., Henning G. A., Persinger R. y. R., Ricker G. R., 2013, arXiv e-prints, p. arXiv:1306.5333

Georgy C., Ekström S., Granada A., Meynet G., Mowlavi N., Eggenberger P., Maeder A., 2013, A&A, 553, A24

Glagolevskij Y. V., 2007, Astrophysical Bulletin, 62, 244

Gontcharov G. A., 2006, Astronomy Letters, 32, 759

Hauck B., Mermilliod M., 1998, A&AS, 129, 431

Hauck B., North P., 1982, A&A, 114, 23

Hauschildt P. H., Baron E., 1999, Journal of Computational and Applied Mathematics, 109, 41

Hauschildt P. H., Baron E., Allard F., 1997, ApJ, 483, 390

Hensberge H., De Loore C., Zuiderwijk E. J., Hammerschlag-Hensberge G., 1976, A&A, 48, 383

Holdsworth D. L., 2021, Frontiers in Astronomy and Space Sciences, 8, 31

Holdsworth D. L., et al., 2021, MNRAS, 506, 1073

Houk N., Cowley A. P., 1975, University of Michigan Catalogue of two-dimensional spectral types for the HD stars. Volume I. Declinations -90_ to -53_°0.

Houk N., Smith-Moore M., 1988, Michigan Catalogue of Two-dimensional Spectral Types for the HD Stars. Volume 4, Declinations -26°.0 to -12°.0.

Houk N., Swift C., 1999, Michigan Spectral Survey, 5, 0

Husser T. O., Wende-von Berg S., Dreizler S., Homeier D., Reiners A., Barman T., Hauschildt P. H., 2013, A&A, 553, A6

Jenkins J. M., et al., 2016, in Chiozzi G., Guzman J. C., eds, Society of Photo-Optical Instrumentation Engineers (SPIE) Conference Series Vol. 9913, Software and Cyberinfrastructure for Astronomy IV. p. 99133E, doi:10.1117/12.2233418

Khalack V., 2018, MNRAS, 477, 882

Khalack V., LeBlanc F., 2015, AJ, 150, 2

Khalack V., Poitras P., 2015, in New Windows on Massive Stars. pp 383–384

Khalack V., Gallant G., Thibeault C., 2017, MNRAS, 471, 926

Khalack V., et al., 2019, MNRAS, 490, 2102

Khalack V., LeBlanc F., Kobzar O., 2020, in Stellar Magnetism: A Workshop in Honour of the Career and Contributions of John D. Landstreet. pp 201–208 (`arXiv:2003.02936`)

Kobzar O., et al., 2020, in Wade G., Alecian E., Bohlender D., Sigut A., eds, Vol. 11, Stellar Magnetism: A Workshop in Honour of the Career and Contributions of John D. Landstreet. pp 214–218 (`arXiv:2003.05337`)

Kochukhov O., Bagnulo S., 2006, A&A, 450, 763

Kochukhov O., Piskunov N., 2002, A&A, 388, 868

Kochukhov O., Makaganiuk V., Piskunov N., 2010, A&A, 524, A5

Kochukhov O., Rivinius T., Oksala M. E., Romanyuk I., 2011, in Neiner C., Wade G., Meynet G., Peters G., eds, Vol. 272, Active OB Stars: Structure, Evolution, Mass Loss, and Critical Limits. pp 166–171, doi:10.1017/S1743921311010192
Kochukhov O., Johnston C., Alecian E., Wade G. A., BinaMIcS Collaboration 2018, MNRAS, 478, 1749
Kordopatis G., et al., 2013, AJ, 146, 134
Krtička J., Mikulášek Z., Lüftinger T., Jagelka M., 2015, A&A, 576, A82
Kurtz D. W., 1978, Information Bulletin on Variable Stars, 1436, 1
Kurtz D. W., 1981, Information Bulletin on Variable Stars, 1915, 1
Kurtz D. W., Marang F., 1987, MNRAS, 229, 285
Landstreet J. D., 1982, ApJ, 258, 639
Landstreet J. D., Bagnulo S., Andretta V., Fossati L., Mason E., Silaj J., Wade G. A., 2007, A&A, 470, 685
LeBlanc F., Khalack V., Yameogo B., Thibeault C., Gallant I., 2015, MNRAS, 453, 3766
Lenz P., Breger M., 2005, Communications in Asteroseismology, 146, 53
Leone F., 2007, MNRAS, 382, 1690
Leone F., Manfre M., 1996, A&A, 315, 526
Leone F., Catanzaro G., Catalano S., 2000, A&A, 355, 315
Levato H., Malaroda S., Morrell N., Solivella G., Grosso M., 1996, A&AS, 118, 231
Mathys G., 1991, A&AS, 89, 121
Mathys G., 1994, A&AS, 108, 547
Mathys G., 1995, A&A, 293, 746
Mathys G., 2017, A&A, 601, A14
Mathys G., Hubrig S., 1997, A&AS, 124, 475
Michaud G., 1970, ApJ, 160, 641
Michaud G., Alecian G., Richer J., 2015, Atomic Diffusion in Stars, doi:10.1007/978-3-319-19854-5.
Monin D., Bohlender D., Hardy T., Saddlemyer L., 2015, in Nagendra K. N., Bagnulo S., Centeno R., Jesús Martínez González M., eds, None Vol. 305, Polarimetry. pp 191–194, doi:10.1017/S1743921315004755
Napiwotzki R., Schoenberner D., Wenske V., 1993, A&A, 268, 653
Napiwotzki R., et al., 2004, in Hilditch R. W., Hensberge H., Pavlovski K., eds, Astronomical Society of the Pacific Conference Series Vol. 318, Spectroscopically and Spatially Resolving the Components of the Close Binary Stars. pp 402–410 (`arXiv:astro-ph/0403595`)
Ndiaye M. L., LeBlanc F., Khalack V., 2018, MNRAS, 477, 3390
Neiner C., Mathis S., Alecian E., Emeriau C., Grunhut J., BinaMIcS MiMeS Collaborations 2015, in Polarimetry. pp 61–66 (`arXiv:1502.00226`), doi:10.1017/S1743921315004524
Netopil M., Paunzen E., Maitzen H. M., North P., Hubrig S., 2008, A&A, 491, 545
Netopil M., Paunzen E., Hümmerich S., Bernhard K., 2017, MNRAS, 468, 2745
Paunzen E., 2015, A&A, 580, A23
Piskunov N., Kochukhov O., 2002, A&A, 381, 736
Preston G. W., 1972, ApJ, 175, 465
Preston G. W., 1974, ARA&A, 12, 257
Raskin G., et al., 2011, A&A, 526, A69
Renson P., Manfroid J., 1992, A&A, 263, 161
Ricker G. R., et al., 2015, Journal of Astronomical Telescopes, Instruments, and Systems, 1, 014003
Royer F., Grenier S., Baylac M. O., Gómez A. E., Zorec J., 2002, A&A, 393, 897
Rufener F., 1988, Catalogue of stars measured in the Geneva Observatory photometric system : 4 : 1988
Ryabchikova T. A., Landstreet J. D., Gelbmann M. J., Bolgova G. T., Tsymbal V. V., Weiss W. W., 1997, A&A, 327, 1137
Ryabchikova T., et al., 2007, A&A, 462, 1103
Samus' N. N., Kazarovets E. V., Durlevich O. V., Kireeva N. N., Pastukhova E. N., 2017, Astronomy Reports, 61, 80
Shultz M. E., et al., 2018, MNRAS, 475, 5144
Shultz M. E., et al., 2019, MNRAS, 490, 274
Shultz M. E., et al., 2022, arXiv e-prints, p. arXiv:2201.05512
Sichevskij S. G., 2017, Astronomy Reports, 61, 193
Sikora J., Wade G. A., Power J., Neiner C., 2019a, MNRAS, 483, 2300
Sikora J., Wade G. A., Power J., Neiner C., 2019b, MNRAS, 483, 3127
Sikora J., et al., 2019c, MNRAS, 487, 4695
Silvester J., Kochukhov O., Rusomarov N., Wade G. A., 2017, MNRAS, 471, 962
Stassun K. G., et al., 2018, AJ, 156, 102
Stassun K. G., et al., 2019, VizieR Online Data Catalog, p. J/AJ/156/102
Stepien K., 1968, ApJ, 154, 945
Strömgren B., 1966, ARA&A, 4, 433
Torres G., 2010, AJ, 140, 1158
Wade G. A., Donati J. F., Landstreet J. D., Shorlin S. L. S., 2000, MNRAS, 313, 851
Wade G. A., et al., 2016, MNRAS, 456, 2
Watson C. L., Henden A. A., Price A., 2006, Society for Astronomical Sciences Annual Symposium, 25, 47
Wolff S. C., 1981, ApJ, 244, 221
Wraight K. T., Fossati L., Netopil M., Paunzen E., Rode-Paunzen M., Bewsher D., Norton A. J., White G. J., 2012, MNRAS, 420, 757
Zorec J., Royer F., 2012, A&A, 537, A120

APPENDIX A: MAGNETIC FIELD MEASUREMENTS

This paper has been typeset from a TEX/LATEX file prepared by the author.

Table A1. Magnetic field measurements for seven ApBp stars for this study.

Name (HD)	BJD	$\langle B_z \rangle$ G	BJD	$\langle B_z \rangle$ G
10840	Bagnulo et al. (2015)			
	2453184.834907	-174±42		
22920	Borra et al. (1983)		Shultz et al. (2022) (NARVAL)	
	2443736.889	380±140	2458395.67899	487.13 ± 22.66
	2443737.877	200±120	2458386.64070	148.42 ± 17.39
	2443738.847	185±185	2458387.67402	463.73 ± 19.67
	2443740.864	360±180	2458389.66201	188.29 ± 13.15
	Mathys & Hubrig (1997)		Shultz et al. (2022) (ESPaDOnS)	
	2448847.874	351±162	2456557.94247	230.78 ± 11.64
			2456560.95704	481.11 ± 12.22
			2456675.70610	451.58 ± 14.66
			2457437.76397	383.64 ± 15.52
24712	Leone et al. (2000)		Ryabchikova et al. (1997)	
	2451115.558	540±335	2445534.924	1440 ± 170
	2451117.540	530±125	2445535.919	1620 ± 170
	2451118.528	780±210	2445537.907	810 ± 240
	2451119.522	400±360	2445540.929	590 ± 190
	2451120.514	-180±120	2445541.912	500 ± 140
	2451121.520	-225±220	2445543.916	690 ± 260
	2451215.301	355±530	2445544.908	1000± 150
	2451238.257	550±460		
	Wade et al. (2000)		Mathys (1994)	
	2450857.334	610± 43	2447189.549	212±202
	2451192.316	1043± 58	2447190.529	709±236
	2451193.421	653± 86	This study (ESPaDOnS)	
	2451197.362	172± 42	2456559.958	798 ± 20
			2456560.973	897 ± 25
38170	David-Uraz et al. (2021)			
	2458741.145913	-6±25		
	2458743.146673	105±14		
63401	Bagnulo et al. (2015)		This study (ESPaDOnS)	
	2452678.529602	-589±53	2455521.6568	308±65
	2453002.556151	153±95	2457108.2348	-109±58
	2453004.731597	-414±101	2457109.2598	396±60
	2453399.628828	322±55	2457110.2218	339±49
			2457111.2948	-47±23
			2457112.2818	338±54
			2457113.2938	-400±70
74521	Bohlender et al. (1993)		Mathys (1994)	
	2446834.679	770±140	2446894.528	967±121
	2446835.715	640±140	2446895.485	850±128
	2446836.750	580±140	2447279.531	398±190
	2446837.703	500±160	2447280.529	418±156
	2446894.616	200±300	2447281.465	603±107
	Leone (2007)		This study (ESPaDOnS)	
	2453718.717	1032± 30	2457435.932	528± 23
	2453719.710	794± 28	2458437.606	541± 25
			2458457.643	538± 26
77314	This study (dimaPol)			
	2455261.87680	-159±263		
	2455264.79807	259±220		
	2455580.93253	35±205		
	2456678.93416	-291±167		
86592	This study (dimaPol)		This study (dimaPol)	
	2456355.84065	187±755	2457090.87518	1579±143
	2456992.07270	2323±297	2457465.83889	2852±294
	2456995.09549	2098±247	2457476.78068	1613±121
	2457084.84742	2421±181	2458561.81803	664±447
	2457085.87101	505±248	2458562.81450	2080±359
	2457088.84276	551±159	2458563.81851	1190±449
	2457089.84700	1281±174	2458569.79994	873±238